AMERICAN SOCIETY FOR MICROBIOLOGY | Journal of Virology®

VIRUS-CELL INTERACTIONS

MicroRNA 573 Rescues Endothelial Dysfunction during Dengue Virus Infection under PPARγ Regulation

Shefali Banerjee,[a] Chin Wei Xin,[b,c] Justin Jang Hann Chu[b,c]

[a]Department of Biochemistry and Molecular Biology, University of Texas Medical Branch, Galveston, Texas, USA
[b]Department of Microbiology and Immunology, National University of Singapore, Singapore
[c]Infectious Diseases Translational Research Programme, National University of Singapore, Singapore

ABSTRACT Early prognosis of abnormal vasculopathy is essential for effective clinical management of patients with severe dengue. An exaggerated interferon (IFN) response and release of vasoactive factors from endothelial cells cause vasculopathy. This study shows that dengue virus 2 (DENV2) infection of human umbilical vein endothelial cells (HUVEC) results in differentially regulated microRNAs (miRNAs) important for endothelial function. miR-573 was significantly downregulated in DENV2-infected HUVEC due to decreased peroxisome proliferator activator receptor gamma (PPARγ) activity. Restoring miR-573 expression decreased endothelial permeability by suppressing the expression of vasoactive angiopoietin 2 (ANGPT2). We also found that miR-573 suppressed the proinflammatory IFN response through direct downregulation of Toll-like receptor 2 (TLR2) expression. Our study provides a novel insight into miR-573-mediated regulation of endothelial function during DENV2 infection, which can be further translated into a potential therapeutic and prognostic agent for severe dengue patients.

IMPORTANCE We need to identify molecular factors that can predict the onset of endothelial dysfunction in dengue patients. Increase in endothelial permeability during severe dengue infections is poorly understood. In this study, we focus on factors that regulate endothelial function and are dysregulated during DENV2 infection. We show that miR-573 rescues endothelial permeability and is downregulated during DENV2 infection in endothelial cells. This finding can have both diagnostic and therapeutic applications.

KEYWORDS dengue fever, PPARs, endothelial permeability, miR-573

Dengue is an escalating public health concern with 100 to 200 million symptomatic infections occurring annually across the globe (1). Dengue virus (DENV) belongs to *Flaviviridae* family and has four distinct serotypes that are transmitted by the *Aedes* mosquitoes. The disease is usually subclinical or presented with symptoms such as fever, headache, myalgia, and arthralgia in most patients. However, certain patients develop a severe and potentially fatal form of the disease called dengue shock syndrome due to vasculopathy. Increasing trends in urbanization and international travel have contributed to global distribution of the different serotypes, resulting in hyperendemicity and increasing the risk of severe disease, which is more likely during secondary infections by different DENV serotypes (2). Severe dengue is associated with hemodynamic imbalance resulting in excessive plasma leakage in pleural cavities and hypovolemic shock (3). Predicting the onset of severe dengue is clinically challenging, resulting in unnecessary hospitalization and overburdening of the public health care systems, especially in regions of endemicity. The economic burden of the disease is estimated to be US$3 to $4 billion in these regions, highlighting the need for better preventive and diagnostic approaches for efficient clinical management of this disease (4, 5). The current laboratory and clinical markers for predicting the occurrence of severe dengue in patients have paired poorly in clinical settings (6, 7). Designing better

Editor J.-H. James Ou, University of Southern California

Address correspondence to Justin Jang Hann Chu, miccjh@nus.edu.sg.

The authors declare no conflict of interest.

Received 13 December 2021
Accepted 14 January 2022
Published 23 March 2022

diagnostic approaches will require a detailed understanding of the mechanisms contributing to the pathophysiology of the disease.

During severe dengue, antibody-dependent enhancement (8–10), abnormal T cell function (11), platelet activation (12), and mast cell degranulation induce vasoactive mediators, such as TNF-α, VEGF, IP-10, GM-CSF, interleukins (IL-1α, IL-1β, and IL-8), CXCL1, HMGB1, MCP1, and metalloproteinases, which disrupt the endothelial barrier integrity leading to vascular leakage (13). DENV nonstructural protein 1 (NS1) also induces endothelial permeability by directly disrupting the endothelial glycocalyx layer (14). Circulating levels of endothelial activation markers such as sICAM1, sVCAM1, and claudin5, as well as components of the endothelial glycocalyx layer (syndecan and chondroitin sulfate), are elevated in patients with severe dengue, suggesting the involvement of a dysregulated endothelial barrier function (15–19). Patients with severe dengue present with early signs of endothelial dysfunction, as seen by the elevated reactive hyperemia index, which is associated with a 4-fold risk of severe dengue (20). Identifying such factors directly associated with endothelial function during severe dengue is essential and requires focused exploration of endothelial cell function during dengue infection.

MicroRNAs (miRNAs) are a class of small RNAs that have recently been found to be involved in regulating endothelial cell (EC) function (21). miRNAs bind to the 3′ untranslated region (3′ UTR) of target mRNAs and posttranscriptionally regulate protein production (22). miR-125, miR-155, and miR221/222 are some of the miRNAs that are involved in regulating key EC functions such as angiogenesis, inflammation, and permeability (23). Recent studies have also highlighted the role of miRNAs during dengue infection in both *in vitro* and clinical studies (24–27). However, these studies focused on miRNA expression in cells of non-EC origin, and the role of endothelial miRNAs during DENV infection has yet to be explored. Proinflammatory stimuli that regulate EC miRNA expression, especially during vascular pathology, are also common in severe dengue infection (28). Identifying EC miRNAs that regulate pathways associated with inflammation and permeability responses may provide common regulatory networks between the multiple factors mediating EC permeability.

In this study, we show that DENV2 infection of HUVEC resulted in differential regulation of miRNAs involved in EC function. HUVEC have been widely used for vascular pathology studies and are a permissive host for DENV infection (29, 30). Several of the differentially regulated miRNAs were required for maintaining vascular tone and endothelial cell homeostasis. We further elaborated on the role of miR-573 in regulation of endothelial cell function during DENV2 infection. We also provide some preliminary evidence of regulation of miR-573 expression through peroxisome proliferator activator receptor gamma (PPARγ) at the transcriptional level.

RESULTS

DENV2 infection of HUVEC modulates endothelial miRNA expression. Small RNA sequencing was carried out to identify the changes in the miRNA expression profile in HUVEC upon DENV2 infection (MOI of 10). HUVEC have been widely used as an *in vitro* model for vascular studies and are susceptible to DENV infection (29, 30). We identified 188 miRNAs to be differentially regulated during DENV2-infected HUVEC (Fig. 1a). A total of 38 miRNAs from our screen have previously been reported to be differentially regulated during DENV infection of other nonendothelial cell types indicating the robustness of our screen. A complete list of the differentially expressed miRNAs at 24 and 48 h postinfection (hpi) are tabulated in (see Table S1 in the supplemental material). We selected a few of the most highly significant and differentially expressed miRNAs for qRT-PCR analysis, and we observed a similar trend in their expression profiles, further validating the robustness of the sequencing analysis (data not shown). To further complement the RNA-seq data we carried out a mRNA microarray to determine the overall changes in global mRNA expression levels (Fig. 1b). A complete list of the differentially expressed mRNAs is presented in Table S2 in the supplemental material.

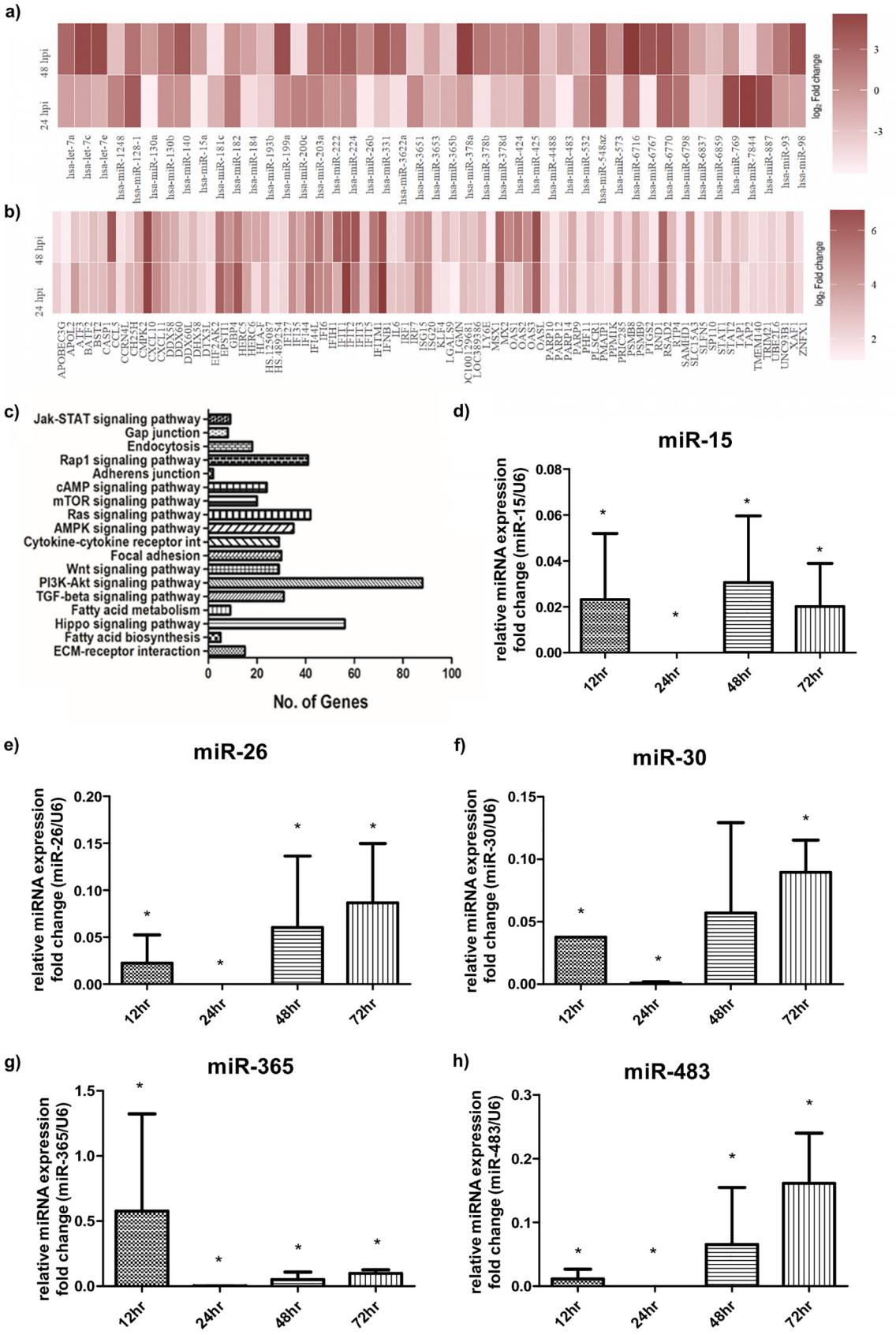

FIG 1 DENV2 infection alters the miRNA expression in HUVEC. (a) Heat map representing the differentially expressed miRNAs in DENV2-infected HUVEC at 24 and 48 hpi. (b) Heat map depicting the overall change in the mRNA expression in response to

(Continued on next page)

TABLE 1 Downregulated miRNAs and their putative mRNA targets

Downregulated miRNA after DENV2 infection	Upregulated mRNAs after DENV2 infection
miR-15	PPM1K, CXCL10
miR-26	PPM1K, KLF4, OAS1, XAF1, EPSTI1, GBP4, STAT1, EIF2AK2, PARP12, SP110, TAP2, PLSCR1, IRF1, ATF3, PARP14, IFIT2, RNF19B, IFI44L, IFIT1, MSX1, IFI35, STAT2, RSAD2, ZNFX1, TRIM25
miR-30	CASP1, GBP4, EIF2AK2, TAP2, OAS2, CXCL10, TRIM5, RNF19B, OASL, BST2, IFI6, TRIM25, APOL2, PPM1K, ETV7, EPSTI1, STAT1, PLSCR1, ATF3, PARP14, IFIT5, STAT2
miR-130	IRF1, CMPK2
miR-365	APOL2, CMPK2, ETV7, GBP4, BATF2, SP110, SAMHD1, SLC15A3, CCL5, IFIT3, IRF1, RNF19B, MX2, IFI44L, IFIT1, LGALS9, DDX60L, LY6E, TRIM25, RND1, PSMB9
miR-483	IRF1, RNF19B, ETV7, OASL, GBP4, SP110, RSAD2, ZNFX1, PSMB9, IFIT3

We superimposed the miRNA and mRNA data sets and identified several putative miRNA-mRNA associations which exhibited a reciprocal relationship in their expression levels. Gene ontology analysis of the differentially regulated miRNA-mRNA targets using Diana miRpath tool (31) identified pathways associated with immune response (JAK-STAT, cytokine, and chemokine signaling), metabolism (Wnt, mTOR, fatty acid synthesis, and PI3-AKT signaling), p53 signaling, and endothelial permeability response (actin cytoskeleton remodeling, gap and tight junctions, adherens junction, and ECM-receptor signaling) (Fig. 1c). We also identified miRNAs, such as miR-15, miR-26, miR-30, miR-365, and miR-483, which regulated mRNAs involved in pathways like gap and tight junctions, adherens junction, and extracellular matrix receptor (ECM receptor) signaling in endothelial cells (32–35). We observed that miR-15 (Fig. 1d), miR-26 (Fig. 1e), miR-30 (Fig. 1f), miR-365 (Fig. 1g), and miR-483 (Fig. 1h) were downregulated in HUVEC at 24 hpi and that some of their putative mRNA targets were upregulated in our microarray data set (Table 1), further emphasizing on the reciprocal relationship between miRNA-mRNA expressions. These observations indicate that DENV2 infection results in an altered miRNA expression profile in endothelial cells that may be responsible for modulating endothelial permeability and activation responses during DENV infection. We also identified miR-573 to be significantly downregulated at 24 hpi, which had putative mRNA targets involved in endothelial permeability and activation responses. Previous reports have shown that miR-573 mitigates the proinflammatory response in a rheumatoid arthritis disease model and has an endothelial protective function (36). We found that miR-573 expression levels were significantly downregulated during DENV2 infection and that the expression levels were inversely proportional to virus titers (Fig. 2a). DENV2 replication kinetics in HUVEC showed peak virus replication between 24 and 72 hpi (data not shown), and a significant decline in miR-573 levels was also observed during this period.

Regulation of miR-573 expression is independent of DENV2 viral replication. We observed that miR-573 was downregulated in DENV2-infected HUVEC at different multiplicities of infection (MOIs of 1, 5, and 10) relative to mock-infected cells (Fig. 2b). We did not observe a significant difference in miR-573 expression in cells infected at different MOIs. To further determine whether miR-573 expression is dependent on active viral replication, HUVEC were treated with an UV-inactivated DENV2 virus. miR-573 expression was reduced in cells treated with the UV-inactivated virus (Fig. 2c). These observations suggest that downregulation of miR-573 expression in DENV2-infected HUVEC is independent of active viral replication. Downregulation of miR-573

FIG 1 Legend (Continued)
DENV2-infection. (c) DIANA mirPath pathway enrichment analysis (Fisher exact test [$P < 0.05$] and false discovery rate [FDR] = 0.01) identified potential pathways regulating endothelial function such as gap junction signaling, tight junction signaling, fatty acid synthesis, etc. (d to h) qRT-PCR analysis of miRNA expression levels for miR-15 (d), miR-26 (e), miR-30 (f), miR-365 (g), and miR-483 (h) during DENV2-infected cells with respect to the mock-infected control. The data represent triplicate biological experiments. A Student *t* test was applied to determine the statistical differences between individual groups (*, $P < 0.05$).

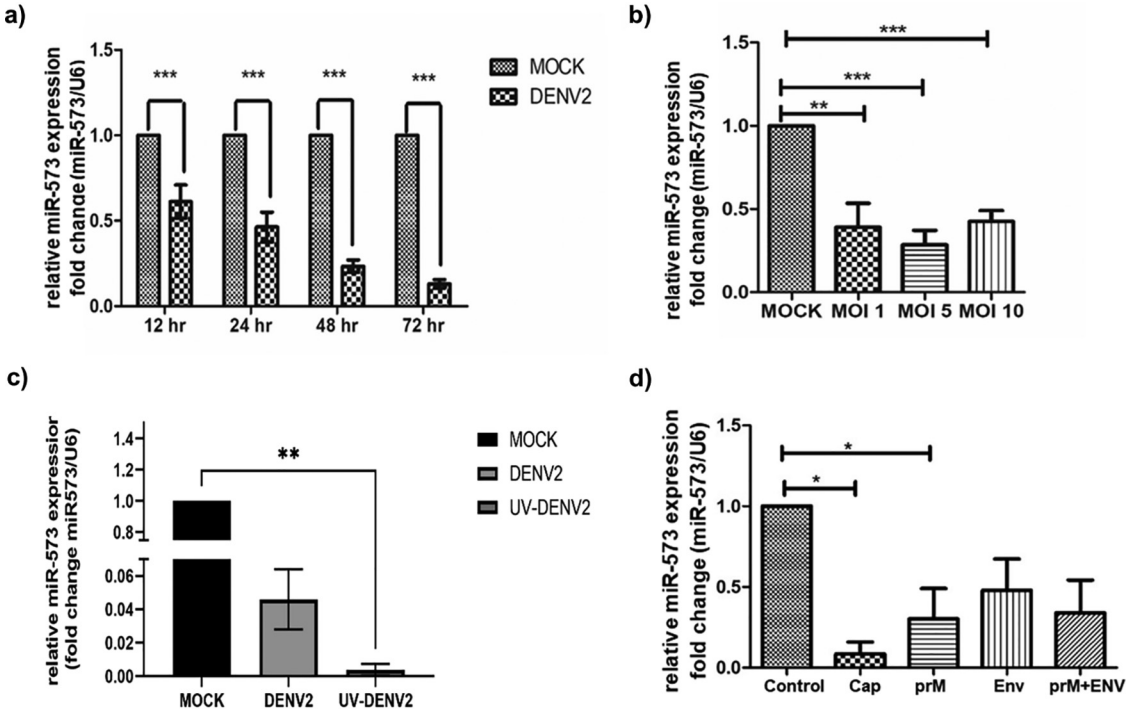

FIG 2 Regulation of miR-573 expression does not directly depend on active viral replication. (a) HUVEC were infected with DENV2 at an MOI of 10, and changes in miR-573 expression levels between mock-infected and virus-infected cells were determined using qRT-PCR at different time intervals postinfection. (b) HUVEC were transfected with DENV2 at different MOIs (1, 5, and 10), and changes in miR-573 expression levels with respect to mock-infected cells were determined using qRT-PCR at 48 hpi. (c) HUVEC were challenged with UV-inactivated DENV2 virus, and 24-hpi miR-573 expression levels were measured relative to mock-infected and DENV2-infected cells by qRT-PCR. (d) HUVEC were transiently transfected with vectors overexpressing different DENV2 structural proteins (capsid [Cap], prM, envelope [Env], and prM+envelope [prM+Env]), and miR-573 expression levels were analyzed 48 h posttransfection using qRT-PCR. Cells transfected with an empty vector backbone were used as a control for all comparisons. Data represent triplicate biological experiments. A Student *t* test was applied to determine the statistical differences between individual groups (*, $P < 0.05$; **, $P < 0.01$).

expression in cells when treated with replication-defective UV-inactivated virus led us to hypothesize whether its expression is modulated by the viral proteins that remain intact upon UV exposure. We transiently transfected HUVEC cells with the recombinant plasmids expressing DENV2 structural proteins (envelope, prM, and capsid proteins) and measured the change in miR-573 expression. We observed a decrease in miR-573 expression for all the three structural proteins and transfection with the capsid construct resulted in greatest downregulation (Fig. 2d) compared to the other constructs. DENV2 capsid protein has been known to interact with host proteins such as HMGB1 and promotes its nuclear to cytoplasmic translocation along with p300/CBP-associated factor (PCAF) acetylase complex (19). Our results indicate that miR-573 downregulation is primarily mediated through virus structural proteins and that the virus capsid protein has the strongest effect.

miR-573 expression is under the transcriptional control of PPARγ. miR-573 is an intergenic miRNA located between DHX15 and PPARγCA1 genes on chromosome 4. We also identified several markers of transcriptionally active regions such as histone modification signals (140 H3K4me3 and H3K27Ac) and DNase1-hypersensitive regions located upstream of miR-573 coding region using the miRStart computational tool (37; data not shown). We identified PPARγ transcription factor binding sites located within 2 kb upstream of miR-573 coding region. PPARγ, which acts as a nuclear hormone receptor, has been shown to suppress the proinflammatory response in endothelial cells in a sepsis disease model (38). We observed a significant reduction in PPARγ protein levels in DENV2-infected HUVEC (Fig. 3a). PPARγ is a ligand-activated transcription factor that, upon activation, undergoes nuclear translocation and binds to the PPAR

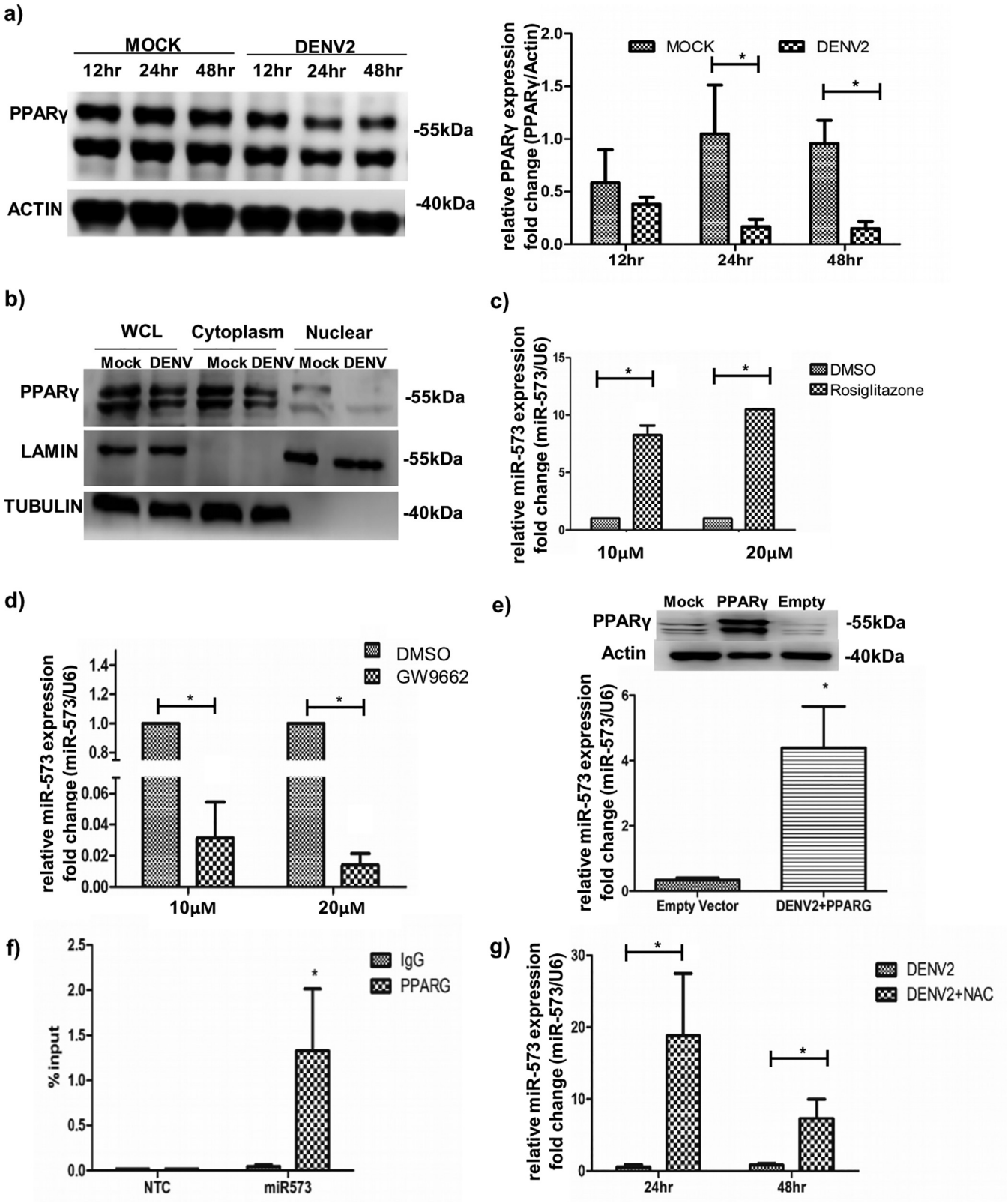

FIG 3 miR-573 expression is under the transcriptional control of PPARγ. (a) Western blot depicting PPARγ expression in mock-infected and DENV2-infected HUVEC at 12, 24, and 48 hpi (left panel). (Right panel) Histogram comparing PPARγ expression in mock-infected and DENV2-infected samples by densitometry. (b) Western blots to determine changes in PPARγ subcellular localization (cytoplasmic and nuclear extracts) in mock-infected and DENV2-infected cells. Whole-cell lysates (WCL) of mock and infected samples were used as controls. (c and d) HUVEC were treated with 10 and 20 μM

(Continued on next page)

response elements (PRE) upstream of its target genes. PPARγ levels in the nuclear fraction of DENV2-infected HUVEC was significantly lower than mock-infected cells (Fig. 3b). To further determine whether modulation of PPARγ activity influences miR-573 transcript levels, HUVEC were treated with various concentrations of rosiglitazone, a PPARγ agonist. A dose-dependent increase in miR-573 expression levels was observed upon rosiglitazone treatment (Fig. 3c). We also observed that treating DENV2-infected cells with rosiglitazone pre- and postinfection resulted in an increase in miR-573 expression, as opposed to solvent-treated cells (data not shown). Inhibiting PPARγ activity with antagonist GW9662 resulted in a dose-dependent decrease in miR-573 expression in HUVEC (Fig. 3d). These observations suggest that miR-573 expression depends on PPARγ activity. Transient overexpression of PPARγ resulted in a significant increase in miR-573 expression in DENV2-infected HUVEC (Fig. 3e). The PPARγ binding site was predicted to be 1,536 bp upstream of miR-573 primary transcript, located between bp 2452178 and bp 24521826 on chromosome 4. We carried out a chromatin immunoprecipitation (ChIP) assay to show direct binding of PPARγ to the predicted site upstream of the miR-573 coding region (Fig. 3f).

Oxidative stress induced during DENV2-infection of HUVEC regulates PPARγ activity. Our results show that PPARγ regulates miR-573 transcription and that DENV2 infection causes a decrease in PPARγ levels. The presence of reactive oxygen species (ROS) has previously been reported to negatively regulate PPARγ expression in endothelial cells (38). Oxidative stress response has also been linked to an indirect decrease in PPARγ activity due to the elimination of endogenous PPARγ ligands from the host cell (38). DENV2 infection also induces an oxidative stress response in host cells (39), and it could be involved in the differential regulation of PPARγ and miR-573 expression in infected cells. To determine whether oxidative stress plays a role in PPARγ expression levels, HUVEC were treated with *N*-acetylcysteine (NAC), which is an aminothiol and acts as a reducing agent, as well as a synthetic precursor of intracellular cysteine and glutathione (GSH) antioxidant system (40). We observed that upon NAC treatment PPARγ protein levels were elevated in DENV2-infected HUVEC (data not shown). Consequently, NAC treatment also resulted in an increase in miR-573 expression during DENV2 infection (Fig. 3g). These findings suggest that regulation of PPARγ activity and its downstream target miR-573 depends on the oxidative stress response induced during DENV2 infection.

Overexpression of miR-573 decreases DENV2-mediated endothelial permeability. Since miR-573 was downregulated during DENV2 infection we further analyzed the effect of miR-573 overexpression on endothelial permeability upon DENV2 infection. HUVEC were transfected with locked nucleic acid (LNA)-modified miR-573 mimic at different concentrations to assess for cytotoxicity, and we observed no significant change in cell viability between mimic-treated and mock-treated cells (Fig. 4a). We also carried out qRT-PCR to confirm overexpression of miR-573 after transfecting the mimic. In comparison to the nontargeting control (NTC)-transfected cells miR-573 expression in mimic-transfected cells was significantly higher (Fig. 4b). miR-573-overexpressing cells were infected with DENV2, and then the permeability characteristics of the endothelial monolayer were assayed. We observed an increase in transendothelial electrical resistance (TEER) in DENV2-infected endothelial monolayer overexpressing miR-573 (Fig. 4c). Similarly, the dextran-FITC influx across the infected monolayer was significantly lower in cells overexpressing miR-573 (Fig. 4d). We also observed a similar effect in miR-573-overexpressing HMEC-1 cells upon DENV2 infection (data not shown). DENV2 infection

FIG 3 Legend (Continued)
rosiglitazone (c), and GW9662 and miR-573 expression was measured relative to solvent (DMSO)-treated cells by qRT-PCR (d). (e) HUVEC were infected with DENV2 at an MOI of 10, and at 24 hpi the cells were transiently transfected with PPARγ overexpression vector and an empty vector, which served as a control. A Western blot shows the overexpression of PPARγ in comparison to the empty vector in infected cells, as well as in mock-infected cells (inset). A bar graph showing differences in miR-573 expression in DENV2-infected cells overexpressing PPARγ relative to the empty vector control. (f) Bar graph showing the level of enrichment of miR-573 expression in PPARγ pulled-down complexes compared to IgG pulled-down chromatin complexes. Fold enrichment was determined relative to position P1, which had no PPARγ binding site. (g) HUVEC were treated with NAC 24 h prior to DENV2 infection, and miR-573 expression levels were determined using qRT-PCR in NAC-treated and untreated infected samples. Data represent triplicate biological experiments. A Student *t* test was applied to determine the statistical differences between individual groups (*, $P < 0.05$).

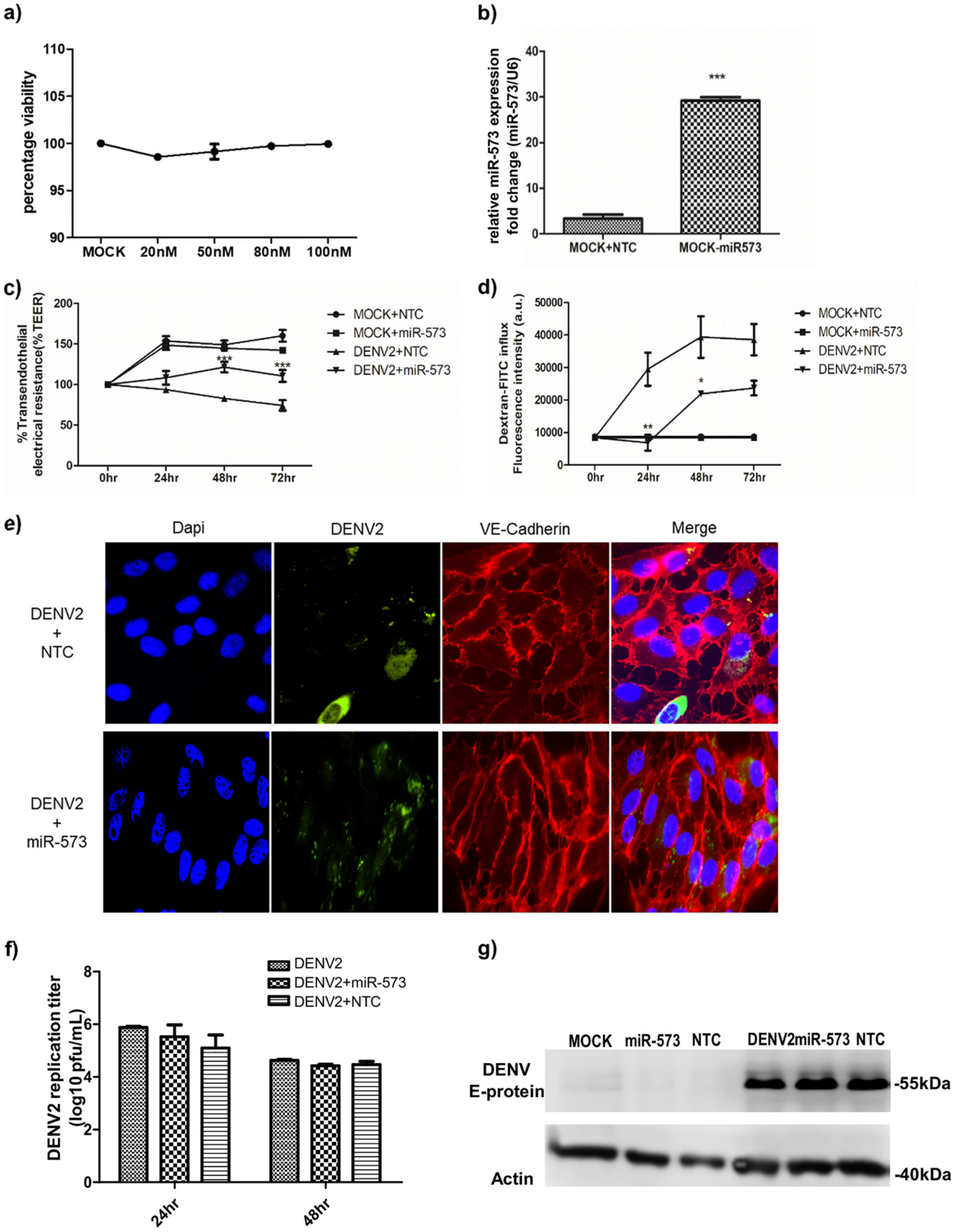

FIG 4 miR-573 reduces endothelial permeability in DENV2-infected HUVEC. (a) HUVEC were transfected with different concentrations of miR-573 mimic (20, 50, 80, and 100 nM), and the cytotoxicity of mimic-treated cells was measured using an Alamar cytotoxicity assay. The percent viability was

(Continued on next page)

of HUVEC results in disorganization of the intercellular adherens junction proteins such as VE-cadherin (30, 41). To determine whether miR-573 overexpression restores the VE-cadherin arrangement in DENV2-infected cells, VE-cadherin protein organization in the infected cells was visualized using immunofluorescence staining. Compared to the NTC-transfected cells, the VE-cadherin proteins were more intact at the intercellular junctions upon miR-573 overexpression (Fig. 4e). Inhibition of miR-573 activity by miR-573 LNA-modified inhibitor resulted in no significant difference between the TEER measurements compared to NTC in DENV2-infected HUVEC (data not shown). No miR-573 binding sites were identified in the DENV2 genome, and miR-573 overexpression had no significant effect on viral protein expression (Fig. 4f) or on viral replication (Fig. 4g). These observations suggest that the rescue in endothelial permeability upon miR-573 overexpression is not mediated through suppression of viral replication but rather through regulation of host factors which are induced upon viral infection.

miR-573 directly represses ANGPT2 expression and modulates endothelial permeability. ANGPT2 is one of the identified miR-573 targets obtained from three individual miRNA target prediction tools (Targetscan, Diana microT-CDS, and miRDB) (42–44). Earlier studies have reported that increase expression of ANGPT2 was responsible for increasing endothelial permeability during DENV2 infection (30, 45). Our study also found that ANGPT2 expression levels were elevated in DENV2-infected HUVEC (data not shown). To determine whether miR-573 binds to the predicted miRNA recognition element (MRE) within the 3′ UTR of ANGPT2, HUVEC were cotransfected with the mimic or the NTC and luciferase constructs carrying wild type or the mutant MRE sequence (Fig. 5a). The luciferase expression in cells carrying the wild-type MRE construct was significantly lower upon miR-573 overexpression with respect to the NTC (Fig. 5a). No significant decrease in luciferase expression levels was observed from the luciferase construct carrying the mutant MRE between cells transfected with miR-573 and the NTC. Similarly, no significant difference was seen in luciferase expression upon inhibition of miR-573 activity for the individual ANGPT2-MRE constructs with respect to NTC (data not shown). ANGPT2 mRNA transcript levels were also downregulated upon miR-573 overexpression (Fig. 5b). miR-573 overexpression resulted in a significant decrease in both intracellular (Fig. 5c) and extracellular (Fig. 5d) ANGPT2 protein levels upon DENV2 infection. To further validate whether the decrease in endothelial permeability observed upon miR-573 overexpression is mediated through suppression of ANGPT2 expression, recombinant ANGPT2 protein was exogenously added to the infected cells overexpressing miR-573. The addition of ANGPT2 resulted in a gradual decrease in TEER measurements in miR-573-overexpressing infected cells (Fig. 5e). Similarly, the dextran-FITC influx significantly increased in miR-573-overexpressing cells after the addition of ANGPT2 (Fig. 5f). These observations suggest that miR-573 binds to the 3′ UTR of ANGPT2 and suppresses its expression, which may contribute to the decrease in endothelial permeability observed upon miR-573 overexpression.

miR-573 regulates the proinflammatory response upon DENV2 infection of HUVEC. To further determine whether miR-573 affects the endothelial activation response in DENV2-infected HUVEC, we measured the secreted levels of proinflammatory cytokines like IL-6, IL-1β, and TNF-α from these cells. In miR-573-overexpressing DENV2-infected HUVEC, the IL-6 levels were significantly reduced compared to NTC

FIG 4 Legend (Continued)
calculated by subtracting the absorbance readings of the treated samples from those of untreated samples. (b) HUVEC were treated with miR-573 (80 nM) or the mimic nontargeting control (NTC, 80 nM) and miR-573 expression was determined by qRT-PCR. HUVEC transfected with the mimic or the nontargeting control were seeded onto the transwell inserts, and the endothelial permeability was measured after mock or DENV2 infection. (c) TEER measurements were compared between mimic-treated and NTC-treated samples for both mock-infected and virus-infected groups. (d) Dextran-FITC influx comparisons were carried out similar to TEER analysis between mimic-treated and NTC-treated samples. (e) VE-cadherin (red) and DENV E-protein (green) were visualized using double immunofluorescence in DENV2-infected HUVEC. (f) Virus titers in DENV2-infected HUVEC treated with miR-573 mimic or the NTC were measured using a plaque assay. No significant difference in viral titers was observed in mimic- and NTC-treated samples. (g) HUVEC transfected with miR-573 or NTC were infected with DENV2 at 24 h posttransfection. Mock-infected controls treated similarly as virus-infected cells were used as controls. Cell lysates were harvested 24 hpi for Western blot analysis of E-protein expression in DENV2-infected and mock-infected cells. Data represent triplicate biological experiments. A Student *t* test was applied to determine the statistical differences between individual groups (*, $P < 0.05$; **, $P < 0.01$; ***, $P < 0.001$).

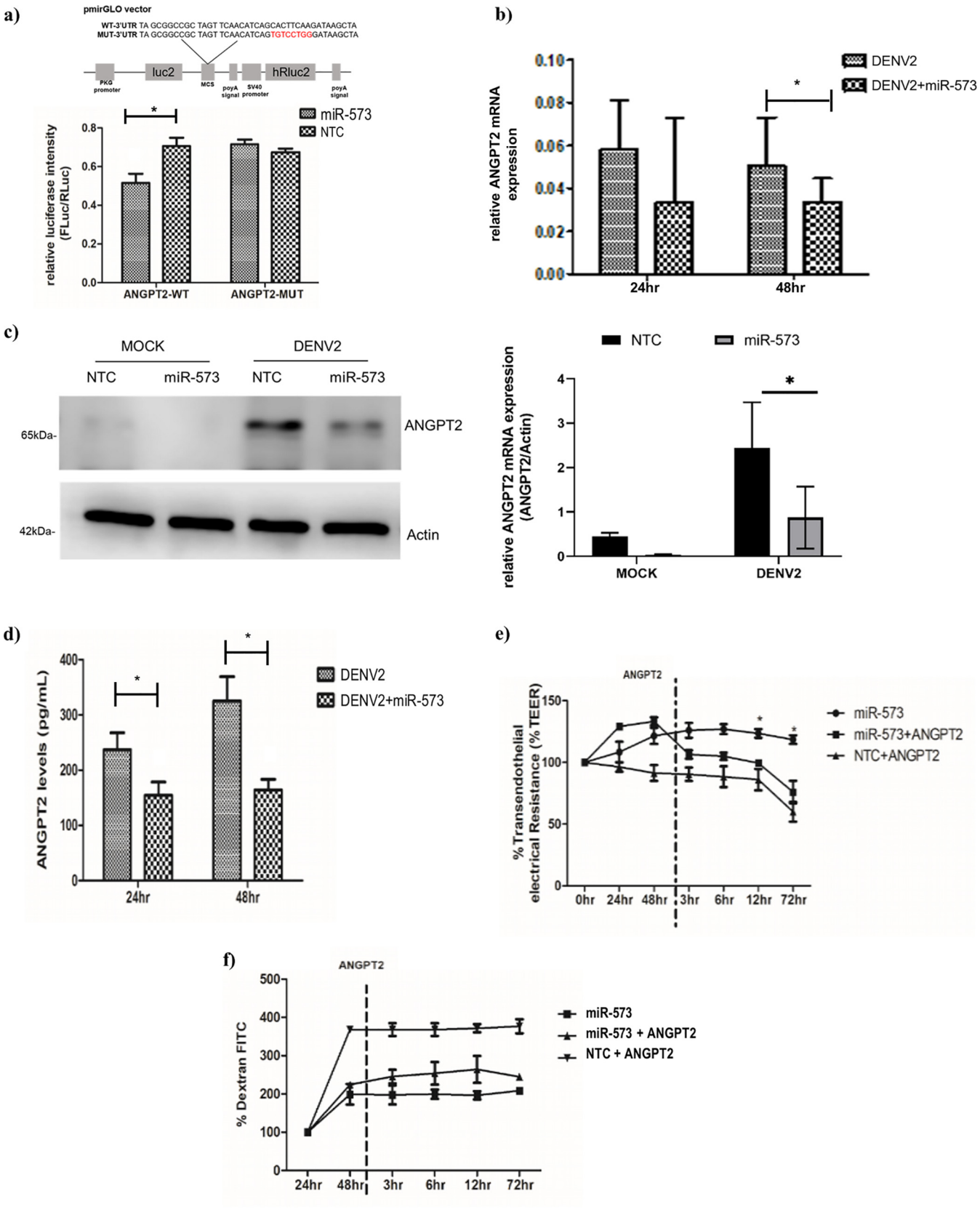

FIG 5 miR-573 targets ANGPT2 expression in DENV2-infected HUVEC. (a) Diagram of the WT-3′ UTR-ANGPT2 and MUT-3′ UTR-ANGPT2 constructs using the backbone of the pmiRGlO dual-luciferase miRNA target expression vector. HUVEC were cotransfected with WT-3′ UTR-ANGPT2 construct and miR-573 mimic (80 nM) or the nontargeting control (NTC-80nM), and the relative luciferase signal intensity (Fluc/Rluc) was measured at 24 h posttransfection.

(Continued on next page)

(Fig. 6a). We did not observe a significant reduction in IL-1β and TNF-α levels between DENV2-infected HUVEC overexpressing miR-573 and the NTC (data not shown). The levels of these cytokines were below the detection limit of even in mock- and DENV2-infected HUVEC in our experimental setup (data not shown). An exaggerated IFN response is responsible for increased endothelial permeability in various proinflammatory diseases (29, 46), and our target prediction analysis found miR-573 to target several of these IFN response genes (Table 2). RSAD2, OAS2, GBP1, etc., have been associated with an exaggerated endothelial activation response (47, 48). The mRNA transcript levels of these IFN response genes were significantly lower in DENV2-infected cells overexpressing miR-573 with respect to NTC (Fig. 6b). Our luciferase reporter assays (as previously described) could not validate any of the predicted miR-573 binding sites for RSAD2, OAS2, and GBP1 (data not shown). Endothelial activation promotes leukocyte transmigration across the monolayer, and we further explored whether miR-573 overexpression reduces leukocyte transmigration across the infected monolayer. Human peripheral blood mononuclear cells (PBMC) were coincubated with HUVEC on transwell inserts and, after 3 h of incubation, the percentage of transmigrating PBMC in the lower chamber was determined by flow cytometry. The percentage of transmigrating CD14- and CD45-positive cells ($CD14^+$ $CD45^+$) across the DENV2-infected monolayer subjected to different treatments—DENV2 infection alone, DENV2-infected with miR-573 mimic, and DENV2-infected with NTC—was evaluated (Fig. 6c and d). A significant decrease in the percentage of the transmigrating PBMC was observed across the DENV2-infected endothelium overexpressing miR-573 compared to the NTC-treated cells (Fig. 6d). Inhibition of miR-573 activity resulted in no significant difference in IL-6 levels and in the percentage of transmigrating PBMC across the DENV2-infected monolayer with respect to NTC (data not shown). Overall, our results indicate that miR-573 overexpression downregulates the endothelial activation response.

miR-573 binds to the 3′ UTR of TLR2 and modulates endothelial activation. Toll-like receptors 2 and 4 (TLR2 and TLR4) were found to be potential predicted targets of miR-573 that also induce IFN response upon activation. TLR2 signaling is responsible for DENV NS1 protein-mediated pathogenesis in DENV (49). We hypothesized that the observed decrease in the type 1 IFN response upon miR-573 overexpression may be a consequence of posttranscriptional repression of TLR2/4 expression. TLR2 expression was elevated in DENV2-infected HUVEC (Fig. 7a). To further validate whether miR-573 binds to the MRE present within the TLR2/4 3′ UTRs, we repeated the luciferase reporter assays with the TLR2/4-MRE constructs. The luciferase expression was significantly lower in HUVEC cells cotransfected with miR-573 and the luciferase construct carrying the wild-type TLR2 MRE sequence (Fig. 7b). Overexpressing miR-573 resulted in a progressive decline in TLR2 protein levels from 26.7 to 58.5% from 24 to 72 hpi (Fig. 7c). However, no significant decrease in luciferase expression was observed for the TLR4-MRE construct under similar conditions (data not shown). No change in TLR4 protein levels was observed in DENV2-infected HUVEC transfected with miR-573 mimic compared to cells transfected with the NTC (Fig. 7d). Therefore, miR-573 only binds to the 3′ UTR of TLR2 and decreases its expression but not to the predicted MRE in the 3′ UTR of TLR4. To further demonstrate that TLR2 is responsible for the increased endothelial activation response, TLR2 receptors were blocked using TLR2 antibody, and the effect on PBMC transmigration across the infected

FIG 5 Legend (Continued)
Luciferase expression was compared between NTC- and mimic-treated samples for the groups expressing the WT or the mutant 3′ UTR construct. HUVEC transfected with miR-573 mimic (80 nM) or the nontargeting control were infected with DENV2 at an MOI of 10, and cell lysates and supernatants were collected at regular time intervals to determine ANGPT2 mRNA and protein expression. (b) Bar graph depicting the relative ANGPT2 mRNA transcript levels in NTC- and mimic-treated groups at 24 and 48 hpi. (c, left panel) Western blot analysis of ANGPT2 protein levels upon miR-573 overexpression in mock- and DENV2-infected samples after 48 hp. (Right panel) Bar graph showing the densitometric analysis of the ANGPT2 protein expression in virus-infected and mock-infected cells treated with the mimic or NTC. (d) HUVEC were transfected with miR-573 mimic or NTC (80 nM) and, at 24 h posttransfection, cells were infected with DENV2 at an MOI of 10. Secreted ANPT2 levels were measured using an enzyme-linked immunosorbent assay (ELISA) at 24 and 48 hpi. A bar graph shows the levels of extracellular ANGPT2 measured by ELISA. (e and f) For rescue experiments, recombinant ANGPT2 (30 ng/mL) was added to the miR-573-overexpressing, DENV2-infected HUVEC monolayer at 48 hpi, and TEER measurements (e) and dextran-FITC influx (f) were determined at regular time intervals and compared to miR-573-treated and NTC-treated infected cells. The data represent triplicate biological experiments. A Student *t* test was applied to determine the statistical differences between individual groups (*, $P < 0.05$).

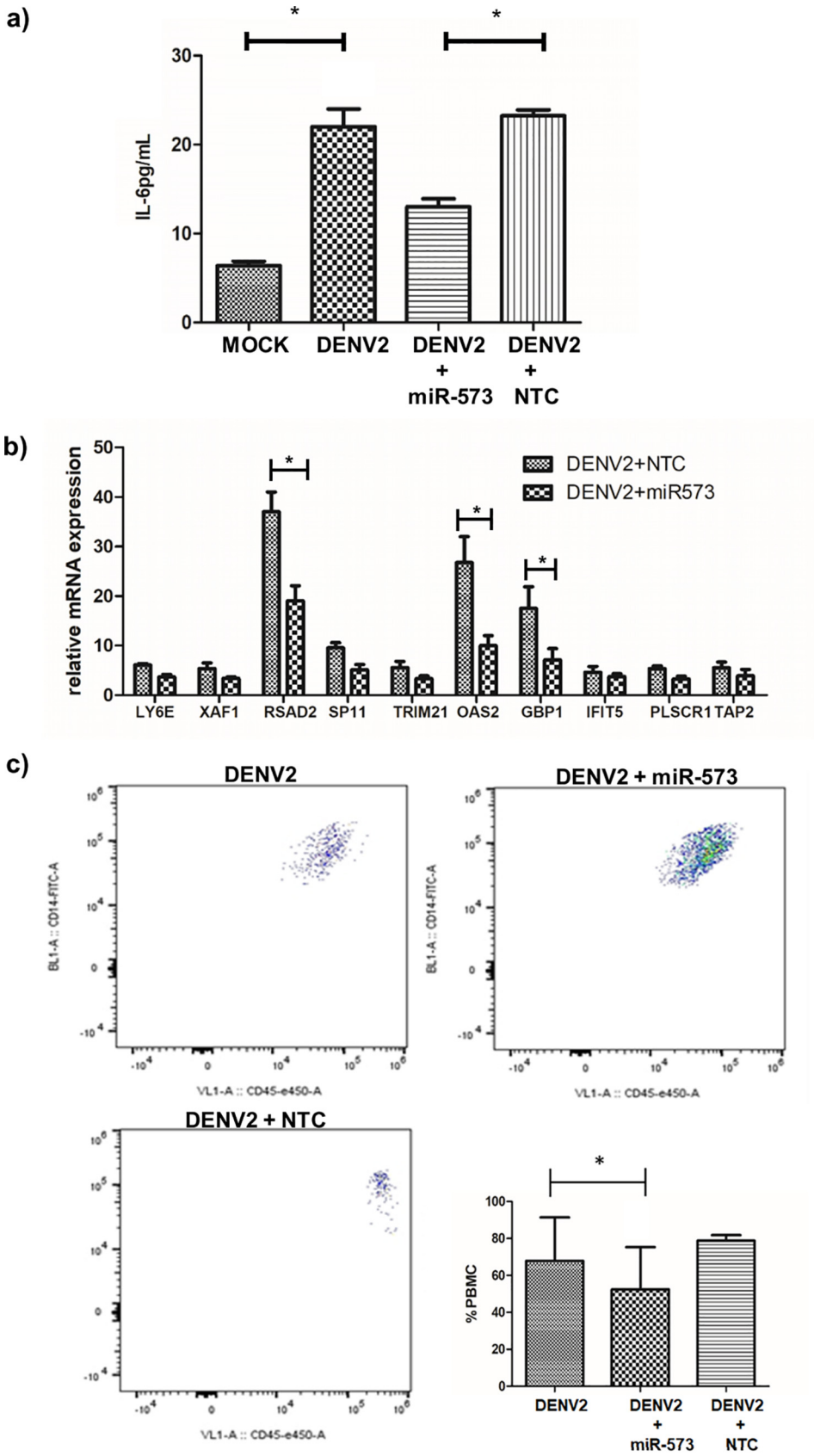

FIG 6 Overexpressing miR-573 suppresses the endothelial activation response. HUVEC were transfected with miR-573 mimic (80 nM) or nontargeting mimic control (NTC, 80 nM) 24 h prior to DENV2 infection

(Continued on next page)

TABLE 2 Gene ontology analysis of miR-573 target genes

Pathway	Genes
Melanoma	AKT2, E2F3, CDH1, EGFR, FGF1, FGF12, FGF13, FGF14, IGF1, NRAS, PDGFC
Pathways in cancer	AKT, APC, CTB2, CBL, E2F3, F2RL3, FOS, GNB4, KIT, SUFU, TRAF1, TRAF3, XIAP, CDH1, CSF1R, CYCS, EDNRB, FGF1, FGF12, FGF13, FGF14, FGF3, FZD8, IGF1, LAMC2, LPAR5, MAPK9, TGFB2, TGFBR1
Rap1 signaling pathway	AKT2, F2RL3, KIT, RAPGEF6, ANGPT2, CDH1, CNR1, CSF1R, EGFR, FGF1, FGF12, FGF13, FGF14, FGFR3, FLT4, IGF1, KDR, LPAR5, MAGI3, MAP2K6, NRAS, PDGFC
Endocytosis	ARF3, ARFGEF1, ASAP1, ASAP3, CBL, GRK7, RAB22A, VPS37A, CAV1, CHMP5, EPS15, EGFR, FGFR3, HSPA1A, HLA-G, SNX2, SPG20, TFRC, TGFBR1, VPS4B, VPS45, VTA1, ZFYEF16
Fructose and mannose metabolism	PFKB4, GMPPB, AKR1B1, ALDOB, FPGT, PFKM
PI3K-Akt signaling pathway	AKT2, GNB4, KIT, MYB, ANGPT2, CREB1, CREB3L4, CHRM2, COL5A1, CSF1R, EGFR, FGF12, FGF1, FGF13, FGF14, FGFR3, FN1, FLT4, GHR, IGF1, KDR, LAMC2, LPAR5, MTCP1, NRAS, PDGFC, PKN2, PPP2R2D, RPS6KB1, TLR2
Alanine, aspartate and glutamate metabolism	ADSL, ALDH5A1, ASPA, GAD2, GLS, GFPT1
Toll-like receptor signaling pathway	AKT2, CXCL9, CD40, CD86, FOS, TRAF3, IRF5, MAPK9, MAP2K6, MAP3K7, TLR2, TLR5, TLR4
Ras signaling pathway	AKT2, ELK1, GNB4, GAB1, KIT, ANGPT2, CSF1R, EGFR, FGF1, FGF12, FGF13, FGFR3, FLT4, IGF1, KDR, KSR2, MAPK9, NRAS, PDGFC, STK4
Toxoplasmosis	AKT2, CD40, XIAP, CYCS, HSPA1A, LAMC2, HLA-DPA1, MAPK9, MAP2K6, MAP3K7, TLR2, TGFB2
Butanoate metabolism	HMGCS1, BDH1, L2HGDH, ALDH5A1, GAD2
Pantothenate and CoA biosynthesis	BCAT1, PANK1, PANK2M, VNN1

monolayer was analyzed. Blocking of TLR2 receptors resulted in a significant decrease in the percentage of transmigrating $CD14^+$ cells across the DENV2-infected monolayer compared to the controls (Fig. 7e). Therefore, the blocking of TLR2 receptors in endothelial cells replicated the similar effect observed during miR-573 overexpression in DENV2-infected HUVEC.

DISCUSSION

Our study was the first to show that DENV2 infection of HUVEC results in differential expression of miRNAs that are potentially involved in regulating endothelial function and immune responses. We also showed that miR-573 reduces endothelial permeability by suppressing the expression of vasoactive ANGPT2 expression during DENV2 infection. It further also suppresses the exaggerated proinflammatory IFN response by downregulating TLR2 expression in DENV2-infected endothelial cells. We also identified that miR-573 was under the direct transcriptional control of nuclear hormone receptor PPARγ, which plays an important role in maintaining endothelial cell function. This study identified a novel mechanism through which miR-573 and PPARγ rescue the endothelial dysfunction observed during DENV2 infection.

Earlier *in vitro* studies in nonendothelial cell types, as well as in dengue patients, have established that DENV infection modulates miRNA expression. However, none of the previous work have looked at the changes in miRNA profiles with respect to endothelial cells. Our study revealed that several miRNAs were downregulated in HUVEC upon DENV2 infection. Earlier studies in Huh7 cells have shown that DENV NS3 and NS4B proteins were responsible for downregulating the major components of the host RNAi machinery, which include the Dicer, Drosha, DGCR8, and Ago proteins (50). Such a shutdown of the RNAi machinery would suppress miRNA biogenesis observed in

FIG 6 Legend (Continued)
(MOI of 10). (a) Secreted levels of IL-6 from mock-infected, DENV2-infected, DENV2+miR573-treated, and DENV2+NTC-treated cells were measured using ELISA at 24 hpi. IL-6 secreted levels were compared to mock-treated cells. (b) HUVEC were transfected with miR-573 mimic and NTC 24 h prior to DENV2 infection and, at 24 hpi, changes in the mRNA transcript levels of endothelial activation markers between NTC-treated and mimic-treated DENV2-infected cells were measured using qRT-PCR. (c) Using the transwell system, HUVEC were transfected with miR-573 mimic and NTC 24 h prior to DENV2 infection. At 24 hpi, 10^6 PBMC were added to the infected monolayer in the transwell insert and at 3 h time interval medium was collected from the lower chamber to determine the percentage of PBMC by flow cytometry. A bar graph depicts the differences in the percentages of PBMC transmigrating across the infected HUVEC monolayer subjected to the different treatments. The data represent triplicate biological experiments. A Student *t* test was applied to determine the statistical differences between individual groups (*, $P < 0.05$).

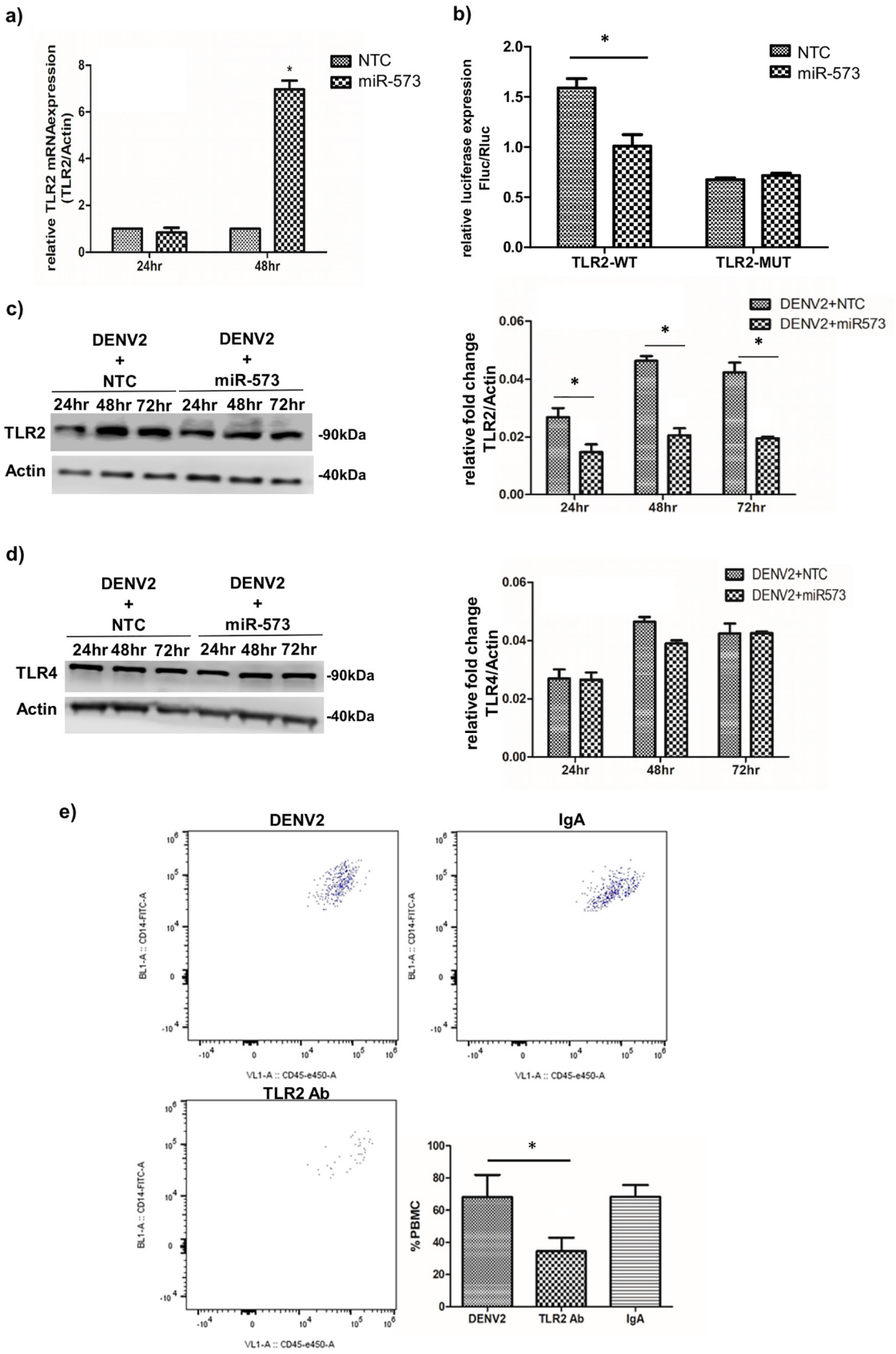

FIG 7 miR-573 targets TLR2 expression and modulates the endothelial activation response in DENV2-infected HUVEC. (a) RNA was harvested from HUVEC infected with DENV2 at an MOI of 10 at 24 and 48 hpi, and TLR2 mRNA expression was determined

(Continued on next page)

DENV2-infected HUVEC as well. However, we did not study the effect of these DENV nonstructural proteins on RNAi machinery, so whether similar mechanisms are in play in DENV2-infected endothelial cells needs to be further examined. Our RNA-seq analysis also identified some of the previously studied miRNAs, such as miR-133a and miR-548g-3p, which directly bind to the 3′ and 5′ UTRs of the DENV genome and regulate virus replication (51, 52). miR-21, miR-30e*, miR-378, miR-146a, miR-223, and the let-7 family of miRNAs have been shown to indirectly regulate viral replication by targeting host factors involved in proinflammatory and innate immune responses (24–26, 51, 53–55). miR-146a, which was also upregulated in DENV2-infected HUVEC, targets TRAF6 expression, subverting the IFN-β and autophagy responses, and enhances DENV replication in monocytes (25, 53). let-7c and miR-21 were also found to be elevated in HUVEC and probably promote DENV replication, as previously explored (26, 54). miR-150, which suppresses SOCS1 expression and promotes a proinflammatory pathogenic response during DENV infection, was also elevated in HUVEC upon DENV2 infection (56). In addition, we also identified miRNAs (miR-26, miR-30, miR-130, miR-365, and miR-483) associated with endothelial function that were differentially regulated in DENV2-infected HUVEC. Interestingly, these miRNAs were significantly downregulated at 24 hpi compared to other time points during infection. We hypothesize that the reduction in miRNA expression may correlate with the increased viral replication at 24 hpi (data not shown). These observations suggest that certain common mechanisms of miRNA-mediated regulation of immune responses might also be at play in both endothelial and nonendothelial cell types during DENV infection.

We further focused on miR-573, which was identified as a potentially important miRNA targeting endothelial functional responses in our gene ontology analysis. miR-573 has previously been explored in the context of different types of cancers with either tumorigenic or antimetastatic function (57–59). miR-573 was also shown to suppress the proinflammatory response in synovial fibroblast cells of rheumatoid arthritis (RASF) thioredoxin domain containing 5 (TXNDC5). Addition of conditioned medium from miR-573-overexpressing RASFs decreases the angiogenic capacity of HUVEC (36). We observed that DENV infection resulted in a decrease in miR-573 expression in HUVEC, which did not show any dependence on the MOI. Infection with a replication defective UV-inactivated virus also resulted in the downregulation of miR-573 expression, which further suggests that its expression does not depend on active viral replication. We observed that transient overexpression of the different DENV structural proteins resulted in the downregulation of miR-573 expression and that the viral capsid protein had the most significant effect. However, we did not observe a dose-dependent response in miR-573 expression in response to the viral capsid protein expression and the other structural proteins (data not shown). We postulate that the presence of DENV2 structural proteins in the cell triggers certain host intrinsic factors, which might be a limiting factor in regulating miR-573 expression (60). In fact, our group has previously shown that DENV2 capsid protein alters HMGB-1 translocation in monocytes initiating a proinflammatory response (61). Though we proposed that miR-573 expression does not depend on active virus replication because both wild-type and UV-inactivated

FIG 7 Legend (Continued)
using qRT-PCR analysis. Mock-infected cells were used as a control. (b) HUVEC were cotransfected with WT-3′ UTR-TLR2 construct and miR-573 mimic (80 nM) or equimolar concentrations of nontargeting control (NTC), and the luciferase signal intensity was measured at 48 h posttransfection. Luciferase expression was compared between the NTC- and mimic-treated samples for the groups expressing WT or mutant 3′ UTR construct. (c) HUVEC were transfected with miR-573 mimic or NTC 24 h prior to DENV2 infection at an MOI of 10, and cell lysates were collected at 24, 48, and 72 hpi for Western blot analyses (left panel). (Right panel) Bar graph depicting the densitometric analysis of the decrease in TLR2 protein expression in miR-573 mimic-transfected cells compared to the NTC. (d) Similarly, a Western blot shows the TLR4 protein expression in DENV2-infected HUVEC cells upon miR-573 overexpression (left panel). (Right panel) Bar graph depicting the densitometric analysis of TLR4 protein expression. (e) HUVEC were seeded on transwell inserts and infected with DENV2 at an MOI of 10. At 24 hpi, the infected cells were treated with 1 μg/mL of anti-TLR2 antibody or IgA (control) and, at 6 h posttreatment, the medium was collected from the lower chamber for flow cytometry analysis. Representative images depict the populations of CD14- and CD45-positive cells in DENV2-infected, TLR2-blocked, and IgA-control cells. A bar graph depicts the percentages of PBMC transmigrating across infected HUVEC monolayers subjected to different treatments. The data represent triplicate biological experiments. A Student *t* test was applied to determine the statistical differences between individual groups (*, $P < 0.05$).

viruses resulted in decrease in miR-573 expression in comparison to mock-infected cells, the observed difference may have resulted from other factors released from infected cells into the medium. To further confirm that miR-573 expression in replication-independent experiments with DENV2 virus-like particles are necessary.

miR-573 is an intergenic miRNA that is located between DHX15 and PPARGCA1 on chromosome 4 with its own transcription regulatory elements. We identified a PPARγ response element (PRE) upstream of the transcription start signal (TSS) in the miR-573 coding region. PPARγ has an endothelial protective function and prevents vascular injury during proinflammatory vascular diseases like sepsis (62, 63), but not much is known about its role during DENV2 infection. DENV2 infection resulted in a decline in PPARγ mRNA, and protein levels and PPARγ activity positively correlated with miR-573 expression in DENV2-infected HUVEC. Treating HUVEC with PPARγ agonists prior to DENV infection resulted in a greater increase in miR-573 transcript levels compared to treating the cells postinfection. No change in miR-573 transcript levels was observed in DENV2-infected cells when they were treated with PPARγ antagonist (data not shown), as opposed to the decline observed in mock-infected cells. The lack of significant decrease in miR-573 expression due to PPARγ antagonism may be attributed to the already low expression of PPARγ and miR-573 in DENV2-infected HUVEC. We further confirmed that transient overexpression of PPARγ in DENV2-infected HUVEC increased miR-573 expression. Furthermore, PPARγ was demonstrated to bind upstream to the miR-573 coding region by a chromatin immunoprecipitation assay. Therefore, these observations suggest that PPARγ positively regulates miR-573 expression at the transcriptional level, and the decrease in PPARγ expression in DENV2-infected HUVEC is probably responsible for the downregulation of miR-573. It has previously been shown that PPARγ expression is affected by the oxidative stress response in endothelial cells induced by proinflammatory stimuli. PPARγ mRNA transcription and activity were inhibited in HUVEC during H_2O_2 exposure, which may be mediated by redox dependent transcription factors such as AP1 (38). DENV2 infection in HUVEC is also associated with an increase in ROS levels, which play a role in endothelial dysfunction (64). We observed that inhibiting ROS production in DENV2-infected HUVEC increases PPARγ and miR-573 expression. Therefore, the ROS imbalance induced during DENV2 infection in HUVEC decreases PPARγ expression, resulting in reduced transcriptional activation of miR-573. However, we observed that at 48 hpi miR-573 expression was reduced, whereas total PPARγ expression remained high in NAC-treated cells. The decrease in miR-573 expression may be attributed to lower levels of PPARγ nuclear translocation. The ROS levels in NAC-treated cells at 48 hpi are probably higher, which might result in reduced PPARγ activity. We further showed that DENV2 structural proteins—and particularly the capsid protein—are responsible for the downregulation of miR-573 expression. We need further experiments to explore whether DENV2 capsid protein induces an oxidative stress response in DENV2-infected HUVEC and downregulates PPARγ and miR-573 expression.

We observed that overexpressing miR-573 in DENV2-infected HUVEC reduces endothelial permeability, as observed with the increase in transendothelial electrical resistance and decrease in dextran-FITC influx. We also observed comparatively more intact VE-cadherin junction complexes in miR-573-overexpressing DENV2-infected HUVEC compared to the NTC-transfected cells. However, immunofluorescence staining of the VE-cadherin complexes is only a qualitative assessment of their organization at interendothelial junctions and would further require higher resolution confocal microscopy to validate these findings. miR-573 had no effect on DENV2 viral replication, suggesting that the decrease in endothelial permeability is not due to decreased viral load and is probably mediated through host factors regulating endothelial function. ANGPT2 was identified as a predicted target of miR-573. Angiopoietins (ANGPT1 and ANGPT2) are endothelial growth factors that regulate endothelial cell homeostasis through Tie receptor tyrosine kinases (45, 65). ANGPT1 is associated with maintaining endothelial cell stability, integrity, and inducing an anti-inflammatory response (45). In contrast,

ANGPT2 antagonizes the protective effect of ANGPT1 signaling by engaging the common Tie2 receptor. Under normal cellular conditions ANGPT1 levels are higher than ANGPT2, and an imbalance in the ANGPT1/ANGPT2 ratio is associated with endothelial dysfunction in vascular inflammatory diseases such as sepsis (45). Both *in vitro* and clinical studies have shown that, during DENV2 infection, ANGPT2 levels are elevated, resulting in a skewed ANGPT1/ANGPT2 ratio (30, 66). An increase in ANGPT2 expression is associated with disorganized VE-cadherin complexes at intercellular junctions in the endothelium (65). In addition, under proinflammatory conditions, ANGPT2 induces the formation of actin stress fibers, resulting in EC contractility, and destabilizes EC-ECM adhesion through $\alpha 5\beta 1$ integrin signaling (67). The factors responsible for the elevated ANGPT2 expression are less explored. miR-573 was predicted to bind to the miRNA response element (MRE) present in the 3′ UTR of ANGPT2. In addition, the expression levels of miR-573 and ANGPT2 were negatively correlated. miR-573 was shown to bind to the 3′ UTR of ANGPT2 in a luciferase reporter construct, which resulted in decreased luciferase expression. Overexpressing miR-573 suppressed ANGPT2 expression and reduced the secreted levels of ANGPT2 from DENV2-infected HUVEC. Furthermore, addition of recombinant ANGPT2 protein to the DENV2-infected cells abrogated the protective effect of miR-573, resulting in increased endothelial permeability. This suggests that the decrease in endothelial permeability mediated by miR-573 was due to the posttranscriptional repression of ANGPT2 protein expression, and the addition of recombinant ANGPT2 protein overcame this repressive effect in infected cells.

miR-573 was also responsible in mitigating the endothelial activation response in DENV2-infected HUVEC. Activated endothelial cells promote leukocyte transcytosis, which further contributes to the local proinflammatory response, thus exacerbating endothelial permeability. Overexpressing miR-573 resulted in decreased expression of proinflammatory cytokines such as IL-6 and IFN response genes, which promote monocyte recruitment and platelet attachment to the activated endothelium. An increase in the circulating levels of IL-6 in patient sera strongly correlates with an increased propensity for developing vascular leakage (68). A reduction in endothelial activation also resulted in a decrease in the percentage of PBMC transmigrating across the DENV2-infected endothelium. Several proinflammatory factors, which are induced by different innate immune mechanisms, increase endothelial activation response in DENV2-infected HUVEC. TLR signaling is an innate immune response mechanism that has been linked to endothelial activation and dysfunction (69–71). TLRs (TLR2, TLR4, and TLR6) are required for DENV2 NS1-induced endothelial activation response (49, 72). Other vasoactive factors, such as HMGB1, IL-1β, TNF-α, histamine, etc., which are significantly elevated during DENV infection, also mediate endothelial permeability via TLR signaling pathways (72, 73). miR-573 was predicted to target the 3′ UTRs of TLR2 and TLR4 that were overexpressed in DENV2-infected HUVEC. *In vitro* studies (as previously described) showed that miR-573 directly binds to the 3′ UTR of TLR2 and decreases its expression at both mRNA and protein level. Although miR-573 resulted in a decrease in luciferase expression in the TLR4 3′ UTR luciferase construct, overexpressing miR-573 did not result in a decrease in TLR4 mRNA and protein expression. Furthermore, blocking of TLR2 in DENV2-infected endothelial cells replicated the effect of miR-573 on IL-6 secretion and PBMC transendothelial migration. These observations suggest that miR-573 suppresses TLR2 expression, thus reducing its surface expression. The lack of availability of TLR2 receptors on the endothelial cell surface regulates the engagement of these limited receptors with vasoactive factors, limiting the endothelial activation response.

The present study shows that miR-573 plays a dual role of reducing the endothelial permeability and activation responses during DENV2 infection. It would be interesting to further explore whether miR-573 exhibits similar endothelial protective function in response to other proinflammatory stimuli, as well as DENV NS1 treatment. Although we did not observe a significant change in mIR-573 expression when HUVEC were exposed to recombinant NS1 treatment (data not shown), since miR-573 reduces TLR2 expression we would expect that overexpressing miR-573 might also reduce NS1-

induced permeability because TLR2 signaling is also involved in NS1-mediated endothelial permeability (49). Further *in vivo* and clinical studies are warranted in order to determine the therapeutic potential of miR-573 in rescuing vascular leakage during severe dengue infection. However, the absence of a miR-573 homologue in mice hampers further *in vivo* studies. An indirect approach of modulating the PPARγ activity to reduce vascular leakage in dengue mouse models can also be explored. PPARγ agonists are already being used as insulin sensitizers in diabetic patients, and their clinical potential is further being explored with respect to other metabolic and inflammatory diseases (74, 75). It would be interesting to explore whether PPARγ agonists can also be repurposed as therapeutic agents to prevent endothelial permeability in dengue patients at risk of developing vascular leakage.

MATERIALS AND METHODS

Virus propagation and *in vitro* infection. DENV2 (strain Den2STp7c6) was propagated in C6/36 cells, and viral titers were quantified by using plaque assays on BHK-21 cells. UV-inactivated virus stock was prepared by exposing the virus stock to UV light for 1.5 h. The UV-inactivated virus in the medium was purified using 100-kDa molecular weight limit centricons (Millipore, UFC910096) and centrifuged at 4,000 $\times$ *g* for 25 min. The UV-inactivated virus was then collected and reconstituted with L-15 medium. The inactivation of the virus by UV irradiation was confirmed by performing a virus plaque assay.

HUVEC (C2517A; Lonza) and HMEC-1 (CRL-3243; ATCC) cells were seeded at 5 $\times$ 10^4 cells/cm^2 density and, upon reaching 80% confluence, were infected with DENV. The cells were infected with 100 μL of L15-medium containing appropriate volumes of either wild-type virus stock or UV-inactivated virus stock to achieve the desired MOI. The infected cells were then incubated at 37°C for 1 h with intermittent shaking at every 15 min. After the incubation period, the cells were washed with sterile phosphate-buffered saline (PBS) and overlaid with EBM-2 medium supplemented with 10% fetal calf serum. The cells were incubated at 37°C with 5% CO_2, and the supernatant containing the virus particles was collected at the desired time points postinfection for plaque assays. All cells used in this study tested negative for mycoplasma contamination using a MycoAlert mycoplasma detection kit (Lonza).

Next-generation miRNA sequencing and microarray analysis. Total RNA from DENV2-infected and mock-infected cells were isolated using a mirVANA RNA isolation kit (Thermo Fisher). The Illumina HiSeq2500 platform was used for miRNA sequencing. Briefly, cDNA libraries for the RNA samples were generated using the TruSeq Small RNA library preparation kit (Illumina). The cDNA libraries were size selected (125 to 175 bp), mixed in equimolar concentrations, and then sequenced using standard TruSeq primer with 50-bp paired end reads. The processed reads were analyzed using for differential miRNA expression, miRNA lists were created using a *P* value cutoff of $<$0.05, with a $>$2-or $<$2-fold change. An Illumina microarray using the Human HT-12 v4.0 BeadChip platform was used for differential gene expression studies. Gene expression data were analyzed using DESeq package (R Bioconductor 3.9), and gene lists were created using a *P* value cutoff of $<$0.05, with a $>$2-or $<$2-fold change. All raw and processed data files have been deposited in the NCBI GEO database (GSE135311).

miRNA LNA mimic, LNA inhibitor, and plasmid transfection. HUVEC cells were reverse transfected with 80 nM miR-573 mimic or equimolar concentrations of cel-miR-39-3p, a mimic negative control (Qiagen) using 4 μM/mL Endoporter reagent (GeneTools, LLC). DENV2 structural proteins were cloned into expression vector from Promega in frame with a C-terminal Flag tag. PPARγ cDNA clone with the C-terminal Flag tag was purchased from (HG12019-CF; Sino Biological). The 3′ UTR luciferase constructs were designed using pmiRGLO Dual luciferase miRNA target expression vector. Wild-type and mutant miRNA target sites were cloned downstream of the Firefly luciferase (luc2) reporter gene in pmirGLO vector (Promega) for luciferase reporter assays. Details of the sequences used for cloning the 3′ UTR are provided in Table S3 in the supplemental material. The plasmid constructs were transfected using the Amaxa 4D-Nucleofector CA-167 (Lonza) protocol.

Endothelial permeability and leukocyte transmigration assays using transwell inserts. HUVEC cells were reverse transfected with 80 nM miR-573 mimic or equimolar concentrations of cel-miR-39-3p as a negative control (NTC) and seeded in transwell inserts (0.3-μm pore; Thincert; Grenier) prior to infection. Transfected cells were infected with DENV2 (MOI of 10) 24 h posttransfection. A mock-infected control transfected with either miR-573 mimic or the NTC was also maintained. Paracellular permeability was assessed by the addition of 0.5 mg/mL fluorescein isothiocyanate-conjugated 70-kDa dextran (dextran FITC; Sigma) to the upper chamber and, after 30 min of incubation at 37°C, 100 μL of medium was removed from the lower chamber and used to measure the fluorescence (490 nm/520 nm). This process was repeated to measure the permeability at the different time points postinfection. The TEER of the HUVEC monolayers was measured with a Millicell-ERS volt-ohmmeter (Millipore) and is reported as the percentage difference between TEER values before and after infection. As previously described, this process was repeated to measure the endothelial electrical resistance at the indicated time points. An empty transwell insert consisting of only medium was maintained as a blank control and was used to determine the permeability of the transwell insert itself. These measurements were subtracted from the observed values of the infected and mock-infected cells.

Leukocyte transmigration assay was carried out by adding 5 $\times$ 10^6 cells/mL hPBMC (catalog no. CC-2702; Lonza) to DENV2-infected HUVEC monolayers in the transwell inserts at 24 hpi. To block TLR2 receptors, DENV2-infected HUVEC were incubated with hTLR2 and IgA isotype control for 30 min. The

monolayer was washed twice with PBS to remove any unbound antibodies prior to the addition of PBMC. After 3 h of incubation at 37°C, medium containing the transmigrated PBMC was collected from the lower chamber and centrifuged at 1,000 × *g* to pellet the PBMCs. The cells were washed with PBS containing 1% bovine serum albumin (BSA) under similar conditions prior to staining with the fluorescently labeled mouse anti-human CD14-FITC (1:500 dilution; Thermo Fisher Scientific, catalog no. 11-0149-42) and mouse anti-human CD45-eFluor (1:500 dilution; Thermo Fisher Scientific, catalog no. 48-0459-42) primary antibodies After a 30-min incubation on ice, the cells were centrifuged at 11,000 × *g* and washed with PBS + 1% BSA twice before fixing with 4% paraformaldehyde at room temperature for 10 min. The cells were then washed and resuspended in 500 μL of PBS. The cells were analyzed using Beckman Coulter CyAn ADP Analyzer. Samples were gated to exclude cell debris.

Real-time qRT-PCR analysis. Total RNA isolated from HUVEC was used for cDNA synthesis prior to PCR amplification. RNA isolation was carried out at the indicated time intervals postinfection. cDNA synthesis was carried out using a miRCURY LNA miRNA RT kit (Qiagen). Briefly, the reverse transcription master mix was prepared on ice by mixing 2 μL of 5× miRCURY RT reaction buffer and 1 μL of 10× miRCURY RT enzyme mix in 5 μL of RNase-free water. Then, 2 μL of template RNA (5 ng/μL) was added to the mixture, making up a final reaction volume of 10 μL. After thorough mixing, the reaction mixture was incubated for 60 min at 42°C for cDNA synthesis. After cDNA synthesis, the reverse transcriptase enzyme was heat inactivated by incubating the complete reaction mixture at 95°C for 5 min. The reaction mixture was then placed on ice and diluted with RNase-free water to 1:60 and used for the following PCR. The PCR mix (for every 10 μL of reaction volume) was prepared by adding 5 μL of 2× miRCURY SYBR green Master Mix (Qiagen) with 0.5 μL of ROX Reference Dye, 1 μL of PCR primer mix, and 3 μL of 1:60-diluted cDNA template. Then, 1 μL of RNase-free water was added to the mixture to make up a final volume to 10 μL. The reaction mixture was thoroughly mixed by pipetting, followed by brief centrifugation prior to PCR amplification on an Applied Biosystems StepOne Plus. The PCR cycling conditions used were as follows: PCR initial heat activation for 2 min at 95°C, followed by denaturation for 10 s at 95°C and then combined annealing and extension at 56°C for 60 s for 40 cycles. Melting-curve analysis was carried out between 60 and 95°C. Data analysis was carried out using software supplied with Applied Biosystems StepOne Plus.

For gene expression analysis one-step qRT-PCR (SYBR green Quantitative RT-PCR kit; Sigma) was carried out. cDNA synthesis was carried out at 42°C for 30 min, followed by denaturation and heat inactivation of RT enzyme at 95°C for 30 s. The PCR cycling conditions used for amplification were as follows: denaturation at 95°C for 5 s, followed by primer annealing at 55°C for 15 s and extension at 72°C for 10 s for 40 cycles. Melting curve analysis was carried out between 60 and 95°C. Data analysis was carried out using the software supplied with Applied Biosystems StepOne Plus.

Protein estimation and indirect immunofluorescence assay. For subcellular fractionation studies, HUVEC were seeded at 5 × 10^4 cells/cm^2 in 10-cm tissue culture-grade plates and lysed using lysis/fractionation buffer after 48 hpi. The lysis buffer, which consists of 20 mM HEPES (pH 7.4), 10 mM KCl, 2 mM $MgCl_2$, 1 mM EDTA, and 1 mM EGTA, was supplemented with 1 mM dithiothreitol and protease inhibitor cocktail (Thermo Fisher Scientific) prior to use. Briefly, 1 mL of lysis buffer was added to the cells, followed by incubation for 15 min on ice to allow complete lysis of the cells. The cell lysates were collected and centrifuged at 720 × *g* for 5 min at 4°C to separate the nuclear and cytoplasmic fractions. The pellet consists of the nuclear fraction, whereas the supernatant comprises of the cytoplasmic fraction. The nuclear pellet was washed twice with 500 μL of lysis buffer by gently dispersing the pellet, followed by centrifugation for 10 min at 720 × *g*. The resulting supernatant was discarded, and the pellet was resuspended in Tris-buffered saline (TBS) containing 0.1% SDS and protease inhibitor before proceeding for sonication (5 s on ice at a power setting of 3). The suspension was sonicated to briefly shear the genomic DNA and homogenize the lysate. Protein estimation of the nuclear and cytoplasmic fractions was carried out using a Bradford assay and then subsequently used for Western blot analysis.

In the experiments that did not require subcellular fractionation, HUVEC were lysed using 1% SDS lysis buffer. Equal amounts of each protein sample were loaded into an SDS-PAGE gel for electrophoretic separation. Proteins were then transferred using the Trans-Blot Turbo transfer system onto a 0.45-μm nitrocellulose membrane (Bio-Rad). The membrane was blocked in TBST buffer containing 5% BSA for 1 h, followed by subsequent washes in 1× TBST buffer and overnight incubation with primary antibody at the appropriate dilution in 5% BSA in TBST. The primary antibodies used were mouse anti-human ANGPT2 (1:500 dilution; R&D Systems), mouse anti-TLR2 (1:500 dilution; Abcam), rabbit anti PPARγ (1:1,000 dilution; Proteintech), and mouse anti-actin (1:10,000; Millipore). After overnight incubation in primary antibody solution, the blots were subjected to three 1× TBST buffer washes for 10 min each. The blots are then probed with the appropriate dilution of secondary antibody in 5% BSA in TBST solution. The secondary antibodies used were HRP-conjugated goat anti-mouse-IgG (1:10,000; Thermo Fisher Scientific) and HRP-conjugated goat anti-rabbit-IgG (1:10,000; Thermo Fisher Scientific). Prior to development, the blots were washed similarly in 1× TBST buffer solution. SuperSignal West Pico chemiluminescent substrate (Thermo Fisher Scientific) was added to the membrane, followed by incubation for 5 min before chemiluminescence detection. The chemiluminescent signal was captured using CL-XPosure film (Thermo Fisher Scientific).

The amount of extracellular ANGPT2 secreted from HUVEC was quantified by using Human Angiopoietin 2 DuoSet ELISA kits (R&D Systems) according to the manufacturer's protocol. The working concentration of ANGPT2 capture antibody was 1 mg/mL. Bradford estimation was carried out, and equal amounts of total protein in the cell culture supernatant were added to each well. Absorbance readings were obtained using an Infinite 200 PRO plate reader (Tecan) at a wavelength of 450 nm with wavelength correction set to 540 nm.

HUVEC were seeded (5 × 10^4 cells/cm^2) onto sterile glass coverslips and infected with DENV2 at an

MOI of 10. Cells were fixed and permeabilized using 4% paraformaldehyde and 0.01% Triton X-100 for 15 min and then washed three times with PBS. The cells were fixed with blocking solution (PBST + 1% BSA) for 30 min at room temperature and then washed with PBS. The fixed cells were stained with primary antibodies against VE-cadherin (mouse anti-human CD144, 1:200; BD Biosciences, catalog no. 555661) and DENV virus (rabbit anti-dengue virus 2, 1:20 dilution; Abcam, catalog no. ab26837). Then, 50 μL of the diluted antibodies was added on a parafilm piece, and the coverslips seeded with HUVEC were inverted with the side containing the cells immersed in the diluted antibodies, followed by incubation for an hour at 37°C in a humidified incubator. After the incubation, the coverslips were then washed in PBS three times and then further incubated with secondary antibodies, such as Dylight 594-conjugated goat anti-mouse IgG (1:1,000 dilution; Thermo Fisher Scientific, catalog no. 35510) and fluorescein isothiocyanate (FITC)-conjugated goat anti-rabbit IgG (1:1,000 dilution; Abcam, catalog no. ab6717). After 1 h of incubation, the cells were washed with PBS, as previously described, and mounted on glass slides in DAPI-containing mounting medium (ProLong Diamond Antifade Mountant). The slides were visualized under the microscope (Olympus) at $\times$1,000 magnification using the Metamorph imaging software program.

Chromatin immunoprecipitation assay. HUVEC were seeded onto 10-cm dishes and, upon reaching confluence (5×10^6 cells), used for a ChIP assay. Briefly, the DNA-protein complexes were cross-linked by dropwise addition of 0.75% formaldehyde to cell culture medium, followed by incubation 10 min at room temperature on a benchtop shaker. Then, 0.125 M glycine was added to the medium to stop the cross-linking reaction. The cross-linked cells were rinsed with 5 mL of ice-cold PBS, scraped off the surface with a cell scraper, and transferred to a 15-mL tube. The cells were centrifuged at 1,000 $\times$ *g* for 5 min at 4°C. The supernatant was aspirated out, and the pellet was resuspended in 500 μL of ChIP lysis buffer. Samples were sonicated to shear DNA to 250 to 1,000 bp. The cell debris was pelleted by centrifugation for 10 min at 4°C and 8,000 $\times$ *g*, and the supernatant containing the chromatin complex was used for immunoprecipitation. Chromatin was incubated with the primary antibody (anti-PPARγ antibody) overnight at 4°C with continuous agitation. Next, 50 μL of protein G-magnetic beads (Millipore) per sample was washed three times with ChIP dilution buffer and added to the chromatin. After 6 h incubation at 4°C, the beads were washed twice with the following buffers: low-salt buffer, high-salt buffer, LiCl, and Tris-EDTA. The beads were resuspended in 250 μL of elution buffer and incubated for 30 min at room temperature with continuous agitation. The eluate was magnetically separated from the beads, and the cross-linking was reversed by overnight incubation with 200 mM NaCl at 65°C. The DNA was purified using QIA quick PCR purification kit (Qiagen) according to the manufacturer's protocol and used for PCR amplification.

SUPPLEMENTAL MATERIAL

Supplemental material is available online only.

SUPPLEMENTAL FILE 1, XLSX file, 0.01 MB.

SUPPLEMENTAL FILE 2, XLSX file, 0.03 MB.

SUPPLEMENTAL FILE 3, XLSX file, 0.01 MB.

ACKNOWLEDGMENTS

This study was supported by a Ministry of Education (MOE), Singapore Tier 2 grant (MOE-2017-358 T2-1-078).

We declare there are no competing financial interests.

REFERENCES

1. Bhatt S, Gething PW, Brady OJ, Messina JP, Farlow AW, Moyes CL, Drake JM, Brownstein JS, Hoen AG, Sankoh O, Myers MF, George DB, Jaenisch T, Wint GRW, Simmons CP, Scott TW, Farrar JJ, Hay SI. 2013. The global distribution and burden of dengue. Nature 496:504–507. https://doi.org/10.1038/nature12060.
2. Guo C, et al. 2017. Global epidemiology of dengue outbreaks in 1990–2015: a systematic review and meta-analysis. Front Cell Infect Microbiol 7:317. https://doi.org/10.3389/fcimb.2017.00317.
3. Deen JL, Harris E, Wills B, Balmaseda A, Hammond SN, Rocha C, Dung NM, Hung NT, Hien TT, Farrar JJ. 2006. The WHO dengue classification and case definitions: time for a reassessment. Lancet 368:170–173. https://doi.org/10.1016/S0140-6736(06)69006-5.
4. Lee J-S, Mogasale V, Lim JK, Carabali M, Lee K-S, Sirivichayakul C, Dang DA, Palencia-Florez DC, Nguyen THA, Riewpaiboon A, Chanthavanich P, Villar L, Maskery BA, Farlow A. 2017. A multi-country study of the economic burden of dengue fever: Vietnam, Thailand, and Colombia. PLoS Negl Trop Dis 11:e0006037. https://doi.org/10.1371/journal.pntd.0006037.
5. Shepard DS, Undurraga EA, Halasa YA. 2013. Economic and disease burden of dengue in Southeast Asia. PLoS Negl Trop Dis 7:e2055. https://doi.org/10.1371/journal.pntd.0002055.
6. Bodinayake CK, Tillekeratne LG, Nagahawatte A, Devasiri V, Kodikara Arachchi W, Strouse JJ, Sessions OM, Kurukulasooriya R, Uehara A, Howe S, Ong XM, Tan S, Chow A, Tummalapalli P, De Silva AD, Østbye T, Woods CW, Gubler DJ, Reller ME. 2018. Evaluation of the WHO 2009 classification for diagnosis of acute dengue in a large cohort of adults and children in Sri Lanka during a dengue-1 epidemic. PLoS Negl Trop Dis 12:e0006258. https://doi.org/10.1371/journal.pntd.0006258.
7. Thanachartwet V, Wattanathum A, Oer-Areemitr N, Jittmittraphap A, Sahassananda D, Monpassorn C, Surabotsophon M, Desakorn V. 2015. Diagnostic accuracy of peripheral venous lactate and the 2009 WHO warning signs for identifying severe dengue in Thai adults: a prospective observational study. BMC Infect Dis 16:46. https://doi.org/10.1186/s12879-016-1386-5.
8. Martina BE. 2014. Dengue pathogenesis: a disease driven by the host response. Sci Prog 97:197–214. https://doi.org/10.3184/003685014X14049173153889.
9. Halstead SB. 2014. Dengue antibody-dependent enhancement: knowns and unknowns. Microbiol Spectr 2. https://doi.org/10.1128/microbiolspec.AID-0022-2014.
10. Guzman MG, Harris E. 2015. Dengue. Lancet 385:453–465. https://doi.org/10.1016/S0140-6736(14)60572-9.

11. Zellweger RM, Eddy WE, Tang WW, Miller R, Shresta S. 2014. CD8$^+$ T cells prevent antigen-induced antibody-dependent enhancement of dengue disease in mice. J Immunol 193:4117–4124. https://doi.org/10.4049/jimmunol.1401597.
12. Ojha A, Nandi D, Batra H, Singhal R, Annarapu GK, Bhattacharyya S, Seth T, Dar L, Medigeshi GR, Vrati S, Vikram NK, Guchhait P. 2017. Platelet activation determines the severity of thrombocytopenia in dengue infection. Sci Rep 7:41697. https://doi.org/10.1038/srep41697.
13. St John AL. 2013. Influence of mast cells on dengue protective immunity and immune pathology. PLoS Pathog 9:e1003783. https://doi.org/10.1371/journal.ppat.1003783.
14. Puerta-Guardo H, Glasner DR, Harris E. 2016. Dengue virus NS1 disrupts the endothelial glycocalyx, leading to hyperpermeability. PLoS Pathog 12:e1005738. https://doi.org/10.1371/journal.ppat.1005738.
15. Liao B, Tang Y, Hu F, Zhou W, Yao X, Hong W, Wang J, Zhang X, Tang X, Zhang F. 2015. Serum levels of soluble vascular cell adhesion molecules may correlate with the severity of dengue virus-1 infection in adults. Emerg Microbes Infect 4:e24. https://doi.org/10.1038/emi.2015.24.
16. Soe HJ, Khan AM, Manikam R, Samudi Raju C, Vanhoutte P, Sekaran SD. 2017. High dengue virus load differentially modulates human microvascular endothelial barrier function during early infection. J Gen Virol 98:2993–3007. https://doi.org/10.1099/jgv.0.000981.
17. Chen H-R, Chao C-H, Liu C-C, Ho T-S, Tsai H-P, Perng G-C, Lin Y-S, Wang J-R, Yeh T-M. 2018. Macrophage migration inhibitory factor is critical for dengue NS1-induced endothelial glycocalyx degradation and hyperpermeability. PLoS Pathog 14:e1007033. https://doi.org/10.1371/journal.ppat.1007033.
18. Suwarto S, Sasmono RT, Sinto R, Ibrahim E, Suryamin M. 2017. Association of endothelial glycocalyx and tight and adherens junctions with severity of plasma leakage in dengue infection. J Infect Dis 215:992–999.
19. Oliveira ERA, Póvoa TF, Nuovo GJ, Allonso D, Salomão NG, Basílio-de-Oliveira CA, Geraldo LHM, Fonseca CG, Lima FRS, Mohana-Borges R, Paes MV. 2017. Dengue fatal cases present virus-specific HMGB1 response in peripheral organs. Sci Rep 7:16011. https://doi.org/10.1038/s41598-017-16197-5.
20. Thein T-L, Wong J, Leo Y-S, Ooi E-E, Lye D, Yeo TW. 2015. Association between increased vascular nitric oxide bioavailability and progression to dengue hemorrhagic fever in adults. J Infect Dis 212:711–714. https://doi.org/10.1093/infdis/jiv122.
21. Qin B, Yang H, Xiao B. 2012. Role of microRNAs in endothelial inflammation and senescence. Mol Biol Rep 39:4509–4518. https://doi.org/10.1007/s11033-011-1241-0.
22. Bartel DP. 2004. MicroRNAs: genomics, biogenesis, mechanism, and function. Cell 116:281–297. https://doi.org/10.1016/S0092-8674(04)00045-5.
23. Aloia AL, Abraham AM, Bonder CS, Pitson SM, Carr JM. 2015. Dengue virus-induced inflammation of the endothelium and the potential roles of sphingosine kinase-1 and microRNAs. Mediators Inflamm 2015:509306. https://doi.org/10.1155/2015/509306.
24. Zhang Y, Zhang Q, Gui L, Cai Y, Deng X, Li C, Guo Q, He X, Huang J. 2018. Let-7e inhibits TNF-alpha expression by targeting the methyl transferase EZH2 in DENV2-infected THP-1 cells. J Cell Physiol 233:8605–8616. https://doi.org/10.1002/jcp.26576.
25. Pu J, Wu S, Xie H, Li Y, Yang Z, Wu X, Huang X. 2017. miR-146a Inhibits dengue-virus-induced autophagy by targeting TRAF6. Arch Virol 162:3645–3659. https://doi.org/10.1007/s00705-017-3516-9.
26. Kanokudom S, Vilaivan T, Wikan N, Thepparit C, Smith DR, Assavalapsakul W. 2017. miR-21 promotes dengue virus serotype 2 replication in HepG2 cells. Antiviral Res 142:169–177. https://doi.org/10.1016/j.antiviral.2017.03.020.
27. Qi Y, Li Y, Zhang L, Huang J. 2013. microRNA expression profiling and bioinformatic analysis of dengue virus-infected peripheral blood mononuclear cells. Mol Med Rep 7:791–798. https://doi.org/10.3892/mmr.2013.1288.
28. Fernandez-Hernando C, Suarez Y. 2018. MicroRNAs in endothelial cell homeostasis and vascular disease. Curr Opin Hematol 25:227–236. https://doi.org/10.1097/MOH.0000000000000424.
29. Warke RV, Xhaja K, Martin KJ, Fournier MF, Shaw SK, Brizuela N, de Bosch N, Lapointe D, Ennis FA, Rothman AL, Bosch I. 2003. Dengue virus induces novel changes in gene expression of human umbilical vein endothelial cells. J Virol 77:11822–11832. https://doi.org/10.1128/jvi.77.21.11822-11832.2003.
30. Ong SP, Ng ML, Chu JJ. 2013. Differential regulation of angiopoietin 1 and angiopoietin 2 during dengue virus infection of human umbilical vein endothelial cells: implications for endothelial hyperpermeability. Med Microbiol Immunol 202:437–452. https://doi.org/10.1007/s00430-013-0310-5.
31. Vlachos IS, Zagganas K, Paraskevopoulou MD, Georgakilas G, Karagkouni D, Vergoulis T, Dalamagas T, Hatzigeorgiou AG. 2015. DIANA-miRPath v3.0: deciphering microRNA function with experimental support. Nucleic Acids Res 43:W460–W466. https://doi.org/10.1093/nar/gkv403.
32. Xu Z, Xiao S-B, Xu P, Xie Q, Cao L, Wang D, Luo R, Zhong Y, Chen H-C, Fang L-R. 2011. miR-365, a novel negative regulator of interleukin-6 gene expression, is cooperatively regulated by Sp1 and NF-κB. J Biol Chem 286:21401–21412. https://doi.org/10.1074/jbc.M110.198630.
33. Qi F, He T, Jia L, Song N, Guo L, Ma X, Wang C, Xu M, Fu Y, Li L, Luo Y. 2015. The miR-30 family inhibits pulmonary vascular hyperpermeability in the premetastatic phase by direct targeting of Skp2. Clin Cancer Res 21:3071–3080. https://doi.org/10.1158/1078-0432.CCR-14-2785.
34. Ye EA, Liu L, Steinle JJ. 2017. miR-15a/16 inhibits TGF-beta3/VEGF signaling and increases retinal endothelial cell barrier proteins. Vision Res 139:23–29. https://doi.org/10.1016/j.visres.2017.07.007.
35. Zhang Y, Qin W, Zhang L, Wu X, Du N, Hu Y, Li X, Shen N, Xiao D, Zhang H, Li Z, Zhang Y, Yang H, Gao F, Du Z, Xu C, Yang B. 2015. MicroRNA-26a prevents endothelial cell apoptosis by directly targeting TRPC6 in the setting of atherosclerosis. Sci Rep 5:9401. https://doi.org/10.1038/srep09401.
36. Wang L, Song G, Zheng Y, Wang D, Dong H, Pan J, Chang X. 2016. miR-573 is a negative regulator in the pathogenesis of rheumatoid arthritis. Cell Mol Immunol 13:839–849. https://doi.org/10.1038/cmi.2015.63.
37. Chien C-H, Sun Y-M, Chang W-C, Chiang-Hsieh P-Y, Lee T-Y, Tsai W-C, Horng J-T, Tsou A-P, Huang H-D. 2011. Identifying transcriptional start sites of human microRNAs based on high-throughput sequencing data. Nucleic Acids Res 39:9345–9356. https://doi.org/10.1093/nar/gkr604.
38. Blanquicett C, Kang B-Y, Ritzenthaler JD, Jones DP, Hart CM. 2010. Oxidative stress modulates PPARγ in vascular endothelial cells. Free Radic Biol Med 48:1618–1625. https://doi.org/10.1016/j.freeradbiomed.2010.03.007.
39. Olagnier D, Peri S, Steel C, van Montfoort N, Chiang C, Beljanski V, Slifker M, He Z, Nichols CN, Lin R, Balachandran S, Hiscott J. 2014. Cellular oxidative stress response controls the antiviral and apoptotic programs in dengue virus-infected dendritic cells. PLoS Pathog 10:e1004566. https://doi.org/10.1371/journal.ppat.1004566.
40. Kerksick C, Willoughby D. 2005. The antioxidant role of glutathione and N-acetyl-cysteine supplements and exercise-induced oxidative stress. J Int Soc Sports Nutr 2:38–44. https://doi.org/10.1186/1550-2783-2-2-38.
41. Dewi BE, Takasaki T, Kurane I. 2008. Peripheral blood mononuclear cells increase the permeability of dengue virus-infected endothelial cells in association with downregulation of vascular endothelial cadherin. J Gen Virol 89:642–652. https://doi.org/10.1099/vir.0.83356-0.
42. Wong N, Wang X. 2015. miRDB: an online resource for microRNA target prediction and functional annotations. Nucleic Acids Res 43:D146–D152. https://doi.org/10.1093/nar/gku1104.
43. Paraskevopoulou MD, Georgakilas G, Kostoulas N, Vlachos IS, Vergoulis T, Reczko M, Filippidis C, Dalamagas T, Hatzigeorgiou AG. 2013. DIANA-microT web server v5.0: service integration into miRNA functional analysis workflows. Nucleic Acids Res 41:W169–W173. https://doi.org/10.1093/nar/gkt393.
44. Agarwal V, Bell GW, Nam J-W, Bartel DP. 2015. Predicting effective microRNA target sites in mammalian mRNAs. Elife 4. https://doi.org/10.7554/eLife.05005.
45. Michels M, van der Ven AJAM, Djamiatun K, Fijnheer R, de Groot PG, Griffioen AW, Sebastian S, Faradz SMH, de Mast Q. 2012. Imbalance of angiopoietin-1 and angiopoetin-2 in severe dengue and relationship with thrombocytopenia, endothelial activation, and vascular stability. Am J Trop Med Hyg 87:943–946. https://doi.org/10.4269/ajtmh.2012.12-0020.
46. Calvert JK, Helbig KJ, Dimasi D, Cockshell M, Beard MR, Pitson SM, Bonder CS, Carr JM. 2015. Dengue virus infection of primary endothelial cells induces innate immune responses, changes in endothelial cells function and is restricted by interferon-stimulated responses. J Interferon Cytokine Res 35:654–665. https://doi.org/10.1089/jir.2014.0195.
47. Afroz S, Giddaluru J, Abbas MM, Khan N. 2016. Transcriptome meta-analysis reveals a dysregulation in extra cellular matrix and cell junction associated gene signatures during Dengue virus infection. Sci Rep 6:33752. https://doi.org/10.1038/srep33752.
48. Pan W, Zuo X, Feng T, Shi X, Dai J. 2012. Guanylate-binding protein 1 participates in cellular antiviral response to dengue virus. Virol J 9:292. https://doi.org/10.1186/1743-422X-9-292.
49. Chen J, Ng MM, Chu JJ. 2015. Activation of TLR2 and TLR6 by dengue NS1 protein and its implications in the immunopathogenesis of dengue virus infection. PLoS Pathog 11:e1005053. https://doi.org/10.1371/journal.ppat.1005053.
50. Kakumani PK, Ponia SS, S RK, Sood V, Chinnappan M, Banerjea AC, Medigeshi GR, Malhotra P, Mukherjee SK, Bhatnagar RK. 2013. Role of RNA interference

(RNAi) in dengue virus replication and identification of NS4B as an RNAi suppressor. J Virol 87:8870–8883. https://doi.org/10.1128/JVI.02774-12.
51. Wen W, He Z, Jing Q, Hu Y, Lin C, Zhou R, Wang X, Su Y, Yuan J, Chen Z, Yuan J, Wu J, Li J, Zhu X, Li M. 2015. Cellular microRNA-miR-548g-3p modulates the replication of dengue virus. J Infect 70:631–640. https://doi.org/10.1016/j.jinf.2014.12.001.
52. Castillo JA, Castrillón JC, Diosa-Toro M, Betancur JG, St Laurent G, Smit JM, Urcuqui-Inchima S. 2016. Complex interaction between dengue virus replication and expression of miRNA-133a. BMC Infect Dis 16:29.
53. Wu S, He L, Li Y, Wang T, Feng L, Jiang L, Zhang P, Huang X. 2013. miR-146a facilitates replication of dengue virus by dampening interferon induction by targeting TRAF6. J Infect 67:329–341. https://doi.org/10.1016/j.jinf.2013.05.003.
54. Escalera-Cueto M, Medina-Martínez I, del Angel RM, Berumen-Campos J, Gutiérrez-Escolano AL, Yocupicio-Monroy M. 2015. Let-7c overexpression inhibits dengue virus replication in human hepatoma Huh-7 cells. Virus Res 196:105–112. https://doi.org/10.1016/j.virusres.2014.11.010.
55. Liu S, Chen L, Zeng Y, Si L, Guo X, Zhou J, Fang D, Zeng G, Jiang L. 2016. Suppressed expression of miR-378 targeting gzmb in NK cells is required to control dengue virus infection. Cell Mol Immunol 13:700–708. https://doi.org/10.1038/cmi.2015.52.
56. Chen R-F, Yang KD, Lee I-K, Liu J-W, Huang C-H, Lin C-Y, Chen Y-H, Chen C-L, Wang L. 2014. Augmented miR-150 expression associated with depressed SOCS1 expression involved in dengue haemorrhagic fever. J Infect 69:366–374. https://doi.org/10.1016/j.jinf.2014.05.013.
57. Chen P, Wang R, Yue Q, Hao M. 2018. Long noncoding RNA TTN-AS1 promotes cell growth and metastasis in cervical cancer via miR-573/E2F3. Biochem Biophys Res Commun 503:2956–2962. https://doi.org/10.1016/j.bbrc.2018.08.077.
58. Wang L, Song G, Tan W, Qi M, Zhang L, Chan J, Yu J, Han J, Han B. 2015. MiR-573 inhibits prostate cancer metastasis by regulating epithelial-mesenchymal transition. Oncotarget 6:35978–35990. https://doi.org/10.18632/oncotarget.5427.
59. Danza K, De Summa S, Pinto R, Pilato B, Palumbo O, Merla G, Simone G, Tommasi S. 2015. MiR-578 and miR-573 as potential players in BRCA-related breast cancer angiogenesis. Oncotarget 6:471–483. https://doi.org/10.18632/oncotarget.2509.
60. Folly BB, Weffort-Santos AM, Fathman CG, Soares LRB. 2011. Dengue-2 structural proteins associate with human proteins to produce a coagulation and innate immune response biased interactome. BMC Infect Dis 11:34. https://doi.org/10.1186/1471-2334-11-34.
61. Ong SP, Lee LM, Leong YFI, Ng ML, Chu JJH. 2012. Dengue virus infection mediates HMGB1 release from monocytes involving PCAF acetylase complex and induces vascular leakage in endothelial cells. PLoS One 7:e41932. https://doi.org/10.1371/journal.pone.0041932.
62. Reddy AT, Lakshmi SP, Kleinhenz JM, Sutliff RL, Hart CM, Reddy RC. 2012. Endothelial cell peroxisome proliferator-activated receptor gamma reduces endotoxemic pulmonary inflammation and injury. J Immunol 189:5411–5420. https://doi.org/10.4049/jimmunol.1201487.
63. Jung Y, Song S, Choi C. 2008. Peroxisome proliferator activated receptor gamma agonists suppress TNFα-induced ICAM-1 expression by endothelial cells in a manner potentially dependent on inhibition of reactive oxygen species. Immunol Lett 117:63–69. https://doi.org/10.1016/j.imlet.2007.12.002.
64. Yacoub S, Lam PK, Huynh TT, Nguyen Ho HH, Dong Thi HT, Van NT, Lien LT, Ha QNT, Le DHT, Mongkolspaya J, Culshaw A, Yeo TW, Wertheim H, Simmons C, Screaton G, Wills B. 2017. Endothelial nitric oxide pathways in the pathophysiology of dengue: a prospective observational study. Clin Infect Dis 65:1453–1461. https://doi.org/10.1093/cid/cix567.
65. Parikh SM. 2013. Dysregulation of the angiopoietin-Tie-2 axis in sepsis and ARDS. Virulence 4:517–524. https://doi.org/10.4161/viru.24906.
66. van de Weg CAM, Pannuti CS, van den Ham H-J, de Araújo ESA, Boas LSV, Felix AC, Carvalho KI, Levi JE, Romano CM, Centrone CC, Rodrigues C. L d L, Luna E, van Gorp ECM, Osterhaus ADME, Kallas EG, Martina BEE. 2014. Serum angiopoietin-2 and soluble VEGF receptor 2 are surrogate markers for plasma leakage in patients with acute dengue virus infection. J Clin Virol 60:328–335. https://doi.org/10.1016/j.jcv.2014.05.001.
67. Hakanpaa L, Sipila T, Leppanen V-M, Gautam P, Nurmi H, Jacquemet G, Eklund L, Ivaska J, Alitalo K, Saharinen P. 2015. Endothelial destabilization by angiopoietin-2 via integrin β1 activation. Nat Commun 6:5962. https://doi.org/10.1038/ncomms6962.
68. Tramontini Gomes de Sousa Cardozo F, Baimukanova G, Lanteri MC, Keating SM, Moraes Ferreira F, Heitman J, Pannuti CS, Pati S, Romano CM, Cerdeira Sabino E. 2017. Serum from dengue virus-infected patients with and without plasma leakage differentially affects endothelial cells barrier function *in vitro*. PLoS One 12:e0178820. https://doi.org/10.1371/journal.pone.0178820.
69. Hilbert T, Dornbusch K, Baumgarten G, Hoeft A, Frede S, Klaschik S. 2017. Pulmonary vascular inflammation: effect of TLR signaling on angiopoietin/TIE regulation. Clin Exp Pharmacol Physiol 44:123–131. https://doi.org/10.1111/1440-1681.12680.
70. Khakpour S, Wilhelmsen K, Hellman J. 2015. Vascular endothelial cell Toll-like receptor pathways in sepsis. Innate Immun 21:827–846. https://doi.org/10.1177/1753425915606525.
71. Johnson RH, Kho DT, O' Carroll SJ, Angel CE, Graham ES. 2018. The functional and inflammatory response of brain endothelial cells to Toll-like receptor agonists. Sci Rep 8:10102. https://doi.org/10.1038/s41598-018-28518-3.
72. Mudaliar H, Pollock C, Ma J, Wu H, Chadban S, Panchapakesan U. 2014. The role of TLR2 and 4-mediated inflammatory pathways in endothelial cells exposed to high glucose. PLoS One 9:e108844. https://doi.org/10.1371/journal.pone.0108844.
73. Huang W, Liu Y, Li L, Zhang R, Liu W, Wu J, Mao E, Tang Y. 2012. HMGB1 increases permeability of the endothelial cell monolayer via RAGE and Src family tyrosine kinase pathways. Inflammation 35:350–362. https://doi.org/10.1007/s10753-011-9325-5.
74. Villapol S. 2018. Roles of peroxisome proliferator-activated receptor gamma on brain and peripheral inflammation. Cell Mol Neurobiol 38:121–132. https://doi.org/10.1007/s10571-017-0554-5.
75. Ivanova EA, Myasoedova VA, Melnichenko AA, Orekhov AN. 2017. Peroxisome proliferator-activated receptor (PPAR) gamma agonists as therapeutic agents for cardiovascular disorders: focus on atherosclerosis. Curr Pharm Des 23:1119–1124. https://doi.org/10.2174/1381612823666161118145850.